Study on Performance and Durability of Fuel Cells Using Hydrocarbon Ionomers

A Doctoral Thesis

Presented to

Green Energy Conversion Science and Technology

Integrated Graduate School of Medicine, Engineering,

and Agricultural Sciences

University of Yamanashi

March 2022

Toshiki Tanaka

Contents

Chapter 1 General Introduction

1.1 Background

In recent years, the rapid development of science and technology has made our lives more comfortable. Along with this, the amount of energy used is increasing year by year, and various energies are produced by thermal power generation, nuclear power generation, etc. to meet these energy demands. Many countries supplement this demand for electricity by consuming large amounts of fossil fuels such as oil, coal, and natural gas. However, the reserves of fossil fuels are finite, and there is concern about their depletion. In addition, mass consumption of fossil fuels emits many harmful substances such as carbon dioxide (CO_2), nitrogen oxides (NOx), and sulfur oxides (SOx), which cause pollution[1-4]. In Japan, due to the 2011 Great East Japan Earthquake, nuclear power generation, which was expected to be used for a long period, is regarded as dangerous, and there is a demand for the development and popularization of sustainable and clean power generation devices that replace existing methods. Currently, renewable energies such as hydropower, wind power, geothermal power, and solar power generation are attracting attention as clean power generation methods, but these power generation methods are affected by the natural environment, so a stable power supply cannot be achieved, and electricity is stored. Needs backup by. In addition, because it requires huge facilities and vast land, it is not always possible to generate electricity in areas where construction sites are limited and electricity is needed. Therefore, it is necessary

to transport electricity by a transmission line, but there is a problem that the loss due to transportation is large. On the other hand, hydrogen has a high energy density and is a renewable energy resource. In addition, stable supply is possible and there is little loss due to transportation. In recent years, fuel cells have been attracting attention as one of the power generation methods using hydrogen. When a fuel cell uses hydrogen as a fuel source, the substance emitted by power generation is mainly water, which is very clean energy that emits almost no harmful substances that affect the environment. Further, since chemical energy is directly converted into electric energy, it is not restricted by the Carnot cycle and waste heat can be used so that it has high energy conversion efficiency. As mentioned above, the fuel cell is a clean and highly efficient power generation device, so it has been actively researched and developed. In 2009, the household fuel cell "ENE-FARM" was introduced to the market, and in 2014, Toyota Motor Corporation. The fuel cell vehicle "MIRAI" has been released to the general public.

1.2 Polymer Electrolyte Fuel Cells (PEFCs)

Among several types of fuel cells, solid polymer fuel cells (PEFCs) are the most studied fuel cells, due to their high power density, quick start-up, and low operating temperature, household fuel cells, and fuel cell vehicles. It has been applied to. The configuration of PEFC is shown in Figure. 1-1. PEFCs are composed of a membrane electrode assembly (MEA) in which both sides of a proton-conducting polymer film that serves as an electrolyte are sandwiched between electrodes consisting of a gas diffusion layer (GDL) and a catalyst layer. NS. GDL is a porous electron conductive support such as carbon paper or carbon cloth and may be treated with polytetrafluoroethylene (PTFE) or the like to make it water repellent for water management in the electrode. The catalyst layer is mainly composed of two materials. One is a Pt-supported carbon catalyst (Pt / CB) in which Pt fine particles of 2-3 nm are highly dispersed on a carbon carrier having a primary particle size of 20-30 nm to increase the surface area of the Pt catalyst. The second is a proton-conducting electrolyte binder, which not only fixes the catalyst on the electrolyte membrane but also coats the Pt / CB surface of the entire catalyst layer to make it a Pt catalyst that does not exist on the electrolyte membrane surface. Can also transport protons, leading to an increase in platinum utilization (Figure 1-2). The hydrogen supplied to the fuel electrode (anode) of PEFC diffuses in the pores of the electrode and is catalyzed on the surface of Pt to be separated into protons (H^+) and electrons (e-). (Eq. 1-1) The generated protons move in the electrolyte

membrane as hydrated ions (hydronium ion $H^+ (H_2O)\ n^+$), and the electrons move to the air electrode (cathode) via an external circuit. Oxygen is supplied to the cathode, and oxygen is reduced by the catalytic action of Pt at the three-phase interface of protons, electrons, and oxygen to generate water. (Eq. 1-2) From the above reactions, the total reaction is as shown in Eq. 1-3.

Anode reaction :	$H_2 \rightarrow 2H^+ + 2e-$	**(Eq. 1-1)**
Cathode reaction :	$1/2O_2 + 2H^+ + 2e- \rightarrow H_2O$	**(Eq. 1-2)**
Cell reaction :	$H_2 + 1/2O_2 \rightarrow H_2O$	**(Eq. 1-3)**

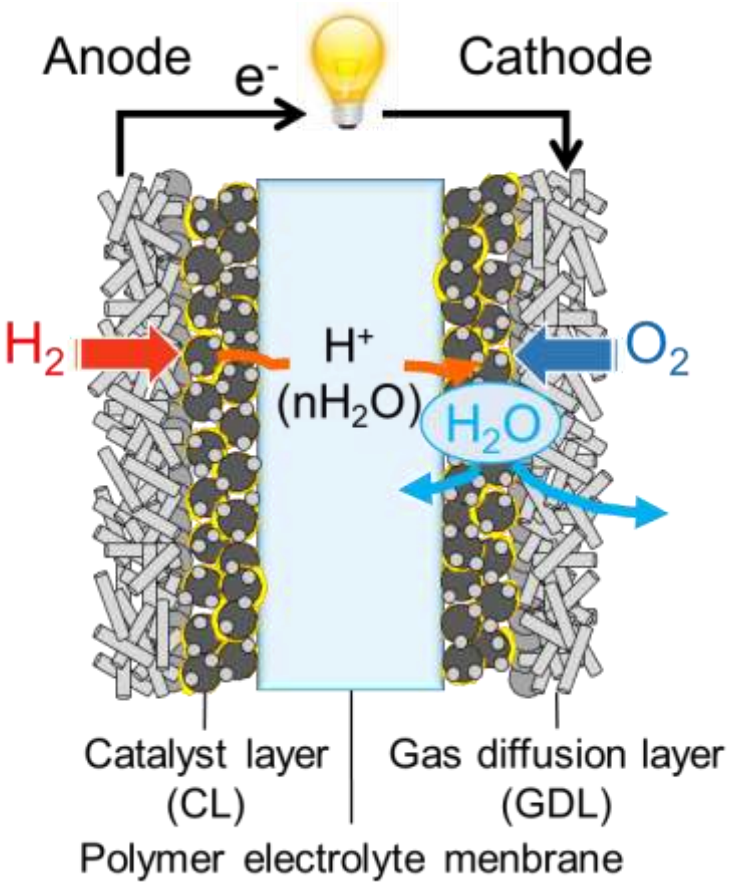

Figure 1-1 Composition of membrane electrode assembly and reaction mechanism

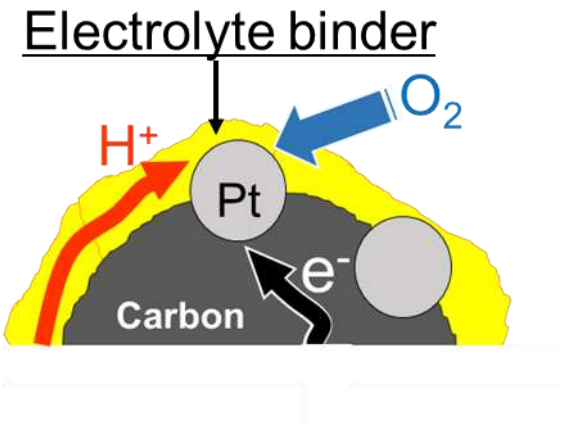

Figure 1-2 Schematic of triple phase boundary on cathode catalyst layer.

The cell potential (E cell) is less than the thermodynamic, reversible potential (E0) due to voltage losses of the open circuit (η_{ocv}), of both anodic and cathodic overpotentials ($\eta_{anode, cathode}$), and ohmic loss (IR_{Ω}). The overpotentials consist of an activation overpotential (η_{act}) and a transport overpotential (η_{tx}). The activation overpotential is dominated by the catalytic activity of the electrodes, in accordance with the Butler-Volmer equation, and transport overpotentials are determined by the mass transport kinetic resistances of O_2, H+, and electrons in the CL, GDL, and membrane, as in Eq. 1-4

$$\mathbf{E_{cell} = E^{\circ} - \eta_{ocv} - \eta_{act,\,anode} - \eta_{tx,\,anode} - \eta_{act,\,cathode} - \eta_{tx,\,cathode} - IR_{\Omega}} \quad \mathbf{(Eq.\ 1\text{-}4)}$$

IR_{Ω} is an overvoltage due to various resistors in the circuit, most of which is derived from the electrolyte membrane. For ηact, the ORR activity of Pt is low, so the overvoltage is significantly higher at the cathode compared to the anode. Therefore, much research has

focused on ORR active catalysts. In addition, at the cathode of ηtx, the water generated by the reaction obstructs the diffusion path of O_2, and the overvoltage increases. Figure 1-3 shows the relationship between each overvoltage and cell voltage.

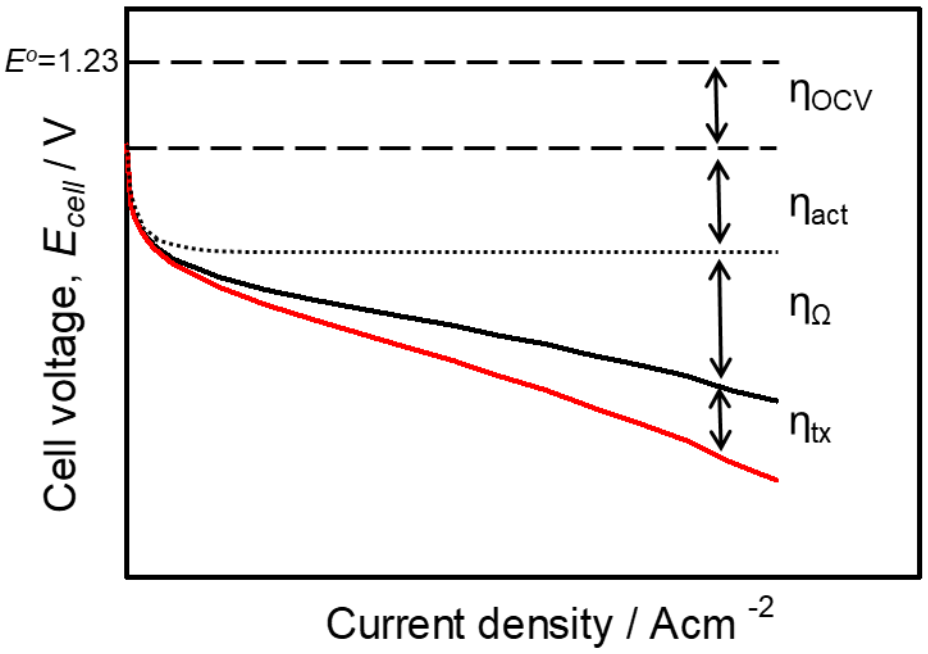

Figure 1-3 Typical polarization curve of PEFC

1.3 Improvement in performance and reliability of PEFCs

As mentioned in the previous section, PEFCs have started to spread, but further improvement in performance and reliability is required for widespread use in the global market. For this purpose, considerable effort has been consumed to develop better-performing proton exchange membranes and electrocatalysts, both of which are major

components of PEFCs[5-8]. Currently, perfluorinated ionomers (eg, Nafion) and their reinforced membranes with porous e -PTFE (eg, GORE SELECT) are state-of-the-art PEMs and most used for commercial PEFCs. Because there is a strong demand for non-fluorinated PEMs with higher thermal stability, lower gas permeability, and potentially lower production cost for next-generation PEFCs[9-11]. In the literature, A number of non-fluorinated PEMs have been reported, such as aromatic polymer-based PEMs[12-17]. Aromatic polymer-based PEMs can be generally prepared via simpler synthetic methods compared to the perfluorinated PEMs, in most cases. The aromatic PEMs have to carry high acid concentration (or ion exchange capacity) in order to have high proton conductivity at low humidity, which eventually causes excessive swelling and dimensional instability at high humidity, resulting in the mechanical failure infrequent wet / dry cycles in operating fuel cells (Figure 1-4). Furthermore, sulfonated poly(phenylene)s[,8, 9] poly(ether ether ketone)s[10], poly(arylene ether sulfone)s[11] and polyimides[12] can be found as proton-exchange membranes in the literature, and some of these have been applied as electrode binders. Inaddition, when hydrocarbon (HC) ionomer is applied to the binder in the catalyst layer, there are various problems such as the catalytic activity decreases due to the interaction (specific adsorption) with the Pt catalyst, and increase the oxygen transport overpotential due to high swelling and low gas permeability. It is very meaningful to investigate ionomers as electrode binders as well as membranes. Focusing on the electrode catalysts, it is well-

known that the carbon support in the cathode catalyst layer corrodes during the cell start-up, most likely due to the high cathode potential (> 1.5 V vs RHE) due to the reverse current reaction caused by the ORR in the anode. Figure 1-5 shows the schematic mechanism of the reverse current reaction. When starting fuel cell operation such as in an automobile, hydrogen, and air happen to directly react in the anode. Accordingly, a carbon oxidation reaction (COR) occurs at the cathode to supply the protons needed for the ORR in the anode degrading the cathode catalyst layer. In the literature, there have been several attempts to address this issue, including the use of more corrosion-resistant catalysts and support materials in the cathode.

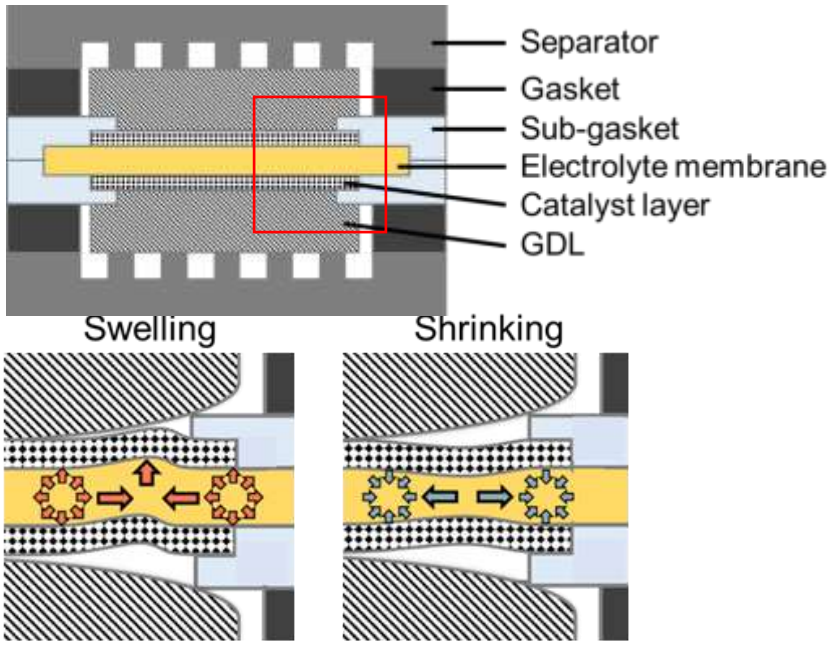

Figure 1-4 Schematic of mechanical failure of ionomer membrane deterioration during wet / dry cycles in fuel cell operation.

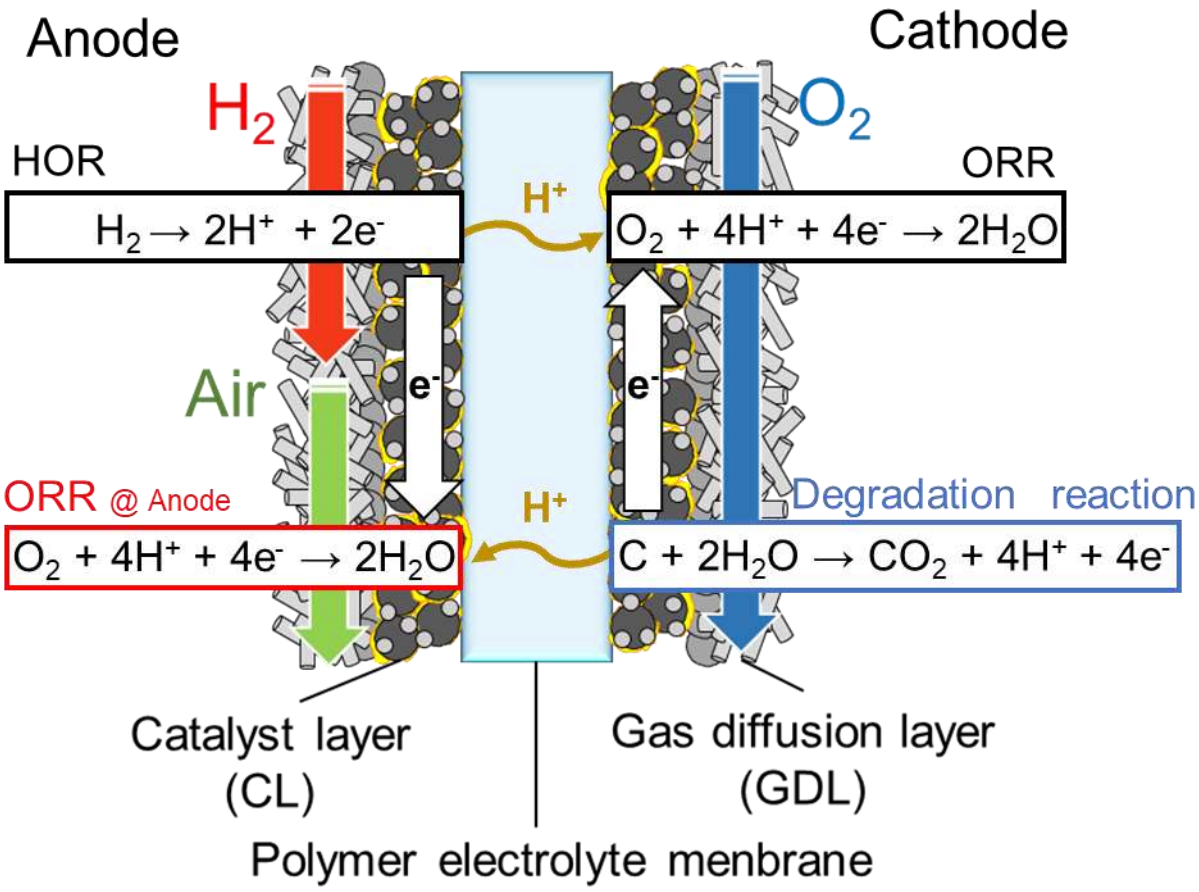

Figure 1-5 Mechanism of reverse current reaction during start-up of a PEFC.

1.4 Objective of this research

As mentioned above, there are still many challenges to fully applying HC-based ionomers to membranes and binders of PEFCs as alternatives to perfluorinated ionomers. This study focuses on HC ionomers membranes and binders aiming at improving the durability of PEFCs. In Chapter 2, the durability of in-house HC ionomer (polyphenylene-based sulfonated ionomer; SPP-QP) membrane against the dry-wet cycles was evaluated using different GDLs. The decomposition mechanism of the membrane during the test was clarified by post-test analyses, e.g., molecular weight measurement at multiple spots and ^{1}H NMR spectra. In Chapter 3, the properties of SPP-QP as electrode binders are discussed. Based on the unique characteristics (specific adsorption) of SPP-QP binder onto the catalysts, the reverse current reaction at the start-up of the fuel cell was mitigated. A cell using SPP-QP or Nafion as a binder was subjected to a gas exchange durability test simulating the start-up of PEFCs. Durability was compared by electrochemical measurement of the cell during the test and the cell performance evaluation before and after the test. Post-test analyses of the cathode catalyst layers using FIB-SIM clarified the deterioration suppression mechanism.

Chapter 4 summarizes the results of the application of HC ionomers to electrolyte membranes and binders and states the prospect of the research.

1.5 Reference

1. BP Statistical Review of World Energy, published by BP global (2016): https://www.bp.com/content/dam/bp/pdf/energy-economics/statistical-review-2016/bp-statistical-review-of-world-energy-2016-full-report.pdf.

2. Intergovernmental Panel on Climate Change fifth Assessment Report (IPCC AR5), published by IPCC: http://www.ipcc.ch/

3. Trend 2015 in Photovoltaic applications, published by International energy agency: http://www.iea-pvps.org/fileadmin/dam/public/report/national/IEA-PVPS_- Trends 20 15 - MedRes.pdf.

4. IEA Wind 2015 Annual Report, published by IEA Wind: https://www.ieawind.org/annual_reports_PDF/2015/2015%20IEA%20Wind%20AR_small.pdf

5. L. Osmieri, J. Park, D. A. Cullen, P. Zelenay, D. J. Myers, K. C. Neyerlin, *Curr. Opin. in Electrochem.*, **25** (2021) 100627.

6. H. Zhang, P.K. Shen, *Chem. Rev.* **112** (2012) 2780-2832.

7. M.P. Rodgers, L. J. Bonville, H. R. Kunz, D. K. Slattery, J. M. Fenton, *Chem. Rev.*, **112** (2012) 6075-6103.

8. W. Liu, T. Suzuki, H. Mao and T. Schmiedel, *J. Electrochem. Soc.* **50** (2013) 51-64.

9. Y. Prykhodko, K. Fatyeyeva, L. Hespel, S. Marais, *Chem. Eng. J.,* **409** (2021) 127329.

10. C.H. Park, C.H. Lee, M.D. Guiver, Y.M. Lee, Prog. *Polym. Sci.*, **36** (2011) 1443-1498.

11. J. Miyake, T. Mochizuki, K. Miyatake, *ACS Macro Lett.* **4** (2015) 750-754.

12. T.J.G. Skalski, M. Adamski, B. Britton, E. M. Schibli, T.J. Peckham, T. Weissbach, T. Mochizuki, S. Lyonnard, B.J. Frisken, S. Holdcroft, *ChemSusChem.*, **11** (2018) 4033−4043.

13. Peressin, N. Adamski, M. Schibli, E. M. Ye, E. Frisken, B. J. Holdcroft, *S. Macromolecules,* **53** (2020) 3119−3138.

14. G. H. Byun, J. A. Kim, N. Y. Kim, Y. S. Cho, C. R. Park, *Mater. Today. Energy*, **17** (2020) 100483.

15. Sutradhar, S. C. Rahman, M. M. Ahmed, F. Ryu, T. Lei, J. Yoon, S. Lee, S. Jin, Y. Kim, *W. J. Power Sources,* **442** (2019) 227233.

16. V.A. Sethuraman, J.W. Weidner, A.T. Haug, L.V. Protsailo, *J. Electrochem. Soc.* **155** (2008) B119-B124.

17. H. Ishikawa, Y. Fujita, J. Tsuji, M. Kusakabe, J. Miyake, Y. Sugawara, K. Miyatake and M. Uchida, *J. Electrochem. Soc.*,**F**(2017) F1204-F1210.

Chapter 2 Wet/dry cycle durability of polyphenylene ionomer membranes in PEFC

2.1 Introduction

For widespread dissemination of PEFCs to the global market, further improvement in performance and reliability, as well as cost reduction, is needed [1,2]. For this purpose, considerable effort has been consumed to develop better-performing electrocatalysts and proton exchange membranes, both of which are major components of PEFCs [3-6]. Currently, perfluorinated ionomers (*e.g.*, Nafion) and their reinforced membranes with porous e-PTFE (*e.g.*, GORE SELECT) are state-of-the-art PEMs and most used for commercial PEFCs because of their excellent proton conductivity and durability under fuel cell operating conditions. There is a strong demand for non-fluorinated PEMs with higher thermal stability, lower gas permeability, and potentially lower production costs for next-generation PEFCs [7-9]. In the literature, a number of non-fluorinated PEMs have been reported, such as aromatic polymer-based PEMs [10-15]. Aromatic polymer-based PEMs can be generally prepared via simpler synthetic methods compared to the perfluorinated PEMs, in most cases. None of them, however, outperform perfluorinated PEMs in terms of proton conductivity and chemical and physical stability. The aromatic PEMs have to carry high acid content (or ion exchange capacity) in order to have high proton conductivity at low humidity, which eventually causes high swelling and dimensional instability at high humidity, resulting in

mechanical failure infrequent wet/dry cycles in fuel cell operation [16]. For example, Ishikawa et al. reported that a sulfonated poly(arylene ether ketone) membrane (SPK) experienced serious damage within only 300 wet/dry cycles. The use of sub-gaskets improved the wet/dry cycle durability of aromatic PEMs, protecting them at the edge of the catalyst layers, where the PEMs tended to experience mechanical damage [17]. The damage was further mitigated by replacing the hard GDL with a soft one. The membrane survived for 30,000 cycles with 2% H_2 leakage after test [18]. More recently, we have developed a novel aromatic PEM (SPP-QP) consisting solely of phenylene rings and sulfonic acid groups. The membrane exhibited high proton conductivity over a wide range of humidity, comparable to that of Nafion, and excellent oxidative stability, thanks to the polyphenylene backbone without heteroatom linkages (*e.g.*, ether bonds) [19.] Furthermore, a reinforced membrane composed of SPP-QP and a porous polyethylene (PE) substrate was prepared to achieve 3,850 cycle-durability in a wet/dry cycle test [20]. In this chapter, I report the mechanical durability of an (unreinforced) SPP-QP membrane evaluated by wet/dry cycle testing in the US-DOE protocol [21], where hydrogen leakage was monitored for up to 30,000 cycles. The effect of gas diffusion layers (hard or soft GDL) was also evaluated. The degradation mechanism was investigated by post-test analyses of the recovered MEAs and membranes, including He leakage testing and molecular weight measurements at multiple spots and ^{1}H NMR spectra.

2.2 Experimental

2.1.1 Preparation of membrane electrode assembly (MEA). SPP-QP membrane (IEC = 2.73 mequiv g^{-1}, 30 μm thick) was prepared according to the literature[19]. A catalyst ink composed of catalyst, ionomer, and solvent was prepared as follows. PtRu/C catalyst (Tanaka Kikinzoku Kogyo, TEC61E54) and PtCo/C catalyst (Tanaka Kikinzoku Kogyo, TEC36E52) were used for the anode and cathode, respectively. Asahi Glass ionomer was used for both catalyst layers. The geometric area of the electrodes was 36 cm^2 (6 cm × 6 cm), and the Pt loading was 0.3 and 0.6 mg cm^{-2} for the anode and cathode, respectively. The catalyst-coated membrane (CCM) was hot-pressed at 160 °C for 5 min. The MEA was prepared by sandwiching the CCM with two commercial gas diffusion layers (hard GDL, 240 μm thick, SGL-25BCH, SGL Carbon Group Co., Ltd.) or two in-house GDLs (soft GDL, 400 μm thick)[18]. A sub-gasket film (38 μm thick) made of poly(phenylene sulfide) was introduced at the edges of both sides. Figure 2-1 shows a schematic of the MEAs. The MEA was mounted into a single cell and sandwiched by two carbon separators equipped with a single serpentine flow path. The cell was tight-sealed by a spring at 10 kgf cm^{-2}.

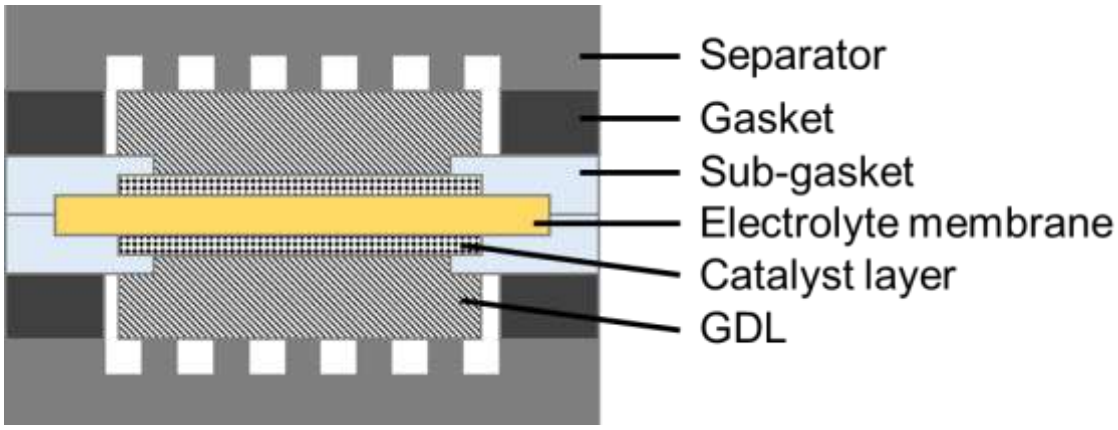

Figure 2-1 Schematic of the MEAs

2.1.2 Wet/dry cycle test. The US DOE protocol[21] shown in Table 2-1 was adopted. At 80 °C of the cell temperature, H_2 was supplied to the anode and N_2 was supplied to the cathode at 2 L min^{-1}. The gas supplied to both electrodes was exchanged between wet (90 ºC of the dew point or 148% RH) and dry at 2-minute intervals.

Table 2-1 Protocol for wet/dry cycle test.

		anode				cathode			
Step	Interval (min)	Gas	Dew point (ºC)	Relative humidity (%)	Flow rate (L min^{-1})	Gas	Dew point (ºC)	Relative humidity (%)	Flow rate (L min^{-1})
1	2	Wet H_2	90	148	2	Wet N_2	90	148	2
2	2	Dry H_2	-50	0.01	2	Dry N_2	-50	0.01	2

2.1.3 H_2 crossover measurement. H_2 crossover was measured to estimate the mechanical degradation of the ionomer membrane during the wet/dry cycle test. The percentage of the H_2 crossing over from the anode to the cathode was calculated from the following equation,

$$H_2\ crossover\ (\%) = \frac{V_{H_2,\text{cathode,outlet}}}{V_{H_2,\text{anode,inlet}}} \times 100 \qquad (1)$$

where $VH_{2,\ anode,\ inlet}$ is the H_2 flow rate at the anode (as dry gas) at 23 °C and 1 atm and $VH_{2,\ cathode,\ outlet}$ is the H_2 flow rate at the cathode outlet. In the measurement of H_2 flow rate at the cathode outlet, the cell temperature, the anode and cathode dew points were set at 60 °C, while H_2 and N_2 were supplied to the anode and cathode at 0.3 L min^{-1}, respectively. The cathode gas was sampled from the outlet and crossover H_2 contained in the cathode gas was quantified by gas chromatography (GC-8A, Shimadzu Co.).

2.1.4 He leak measurement. To evaluate the mechanical degradation of the electrolyte membranes after the wet/dry cycle test, the MEAs were recovered and subjected to He leak test. He was supplied to one side of the MEA and the permeated He was quantified at 36 points by a He detector (UL200Ver.4, INFICON Co., Ltd.) attached to the other side.

2.1.5 Gel permeation chromatography (GPC). The molecular weight of the polymers was measured by gel permeation chromatography with two TOSOH TSKgel α-M and α-3000 columns and a Showa Denko RI-71 differential index detector. N, N-dimethylformamide (DMF) containing 0.05 M LiCl and 0.01% HCl was used as eluent at a flow rate of 0.8 $mLmin^{-1}$. The molecular weight was calibrated with standard polystyrene samples.

2.1.6 Nuclear magnetic resonance (NMR) spectra. ^1H NMR spectra were measured using DMSO-d_6 as a solvent and tetramethyl silane (TMS) as an internal reference at 40 °C using a Bruker DRX-500 spectrometer.

2-3 Results and Discussion

2.3.1 H_2 crossover during wet/dry cycle test. Figure 2-2 shows the amount of H_2 crossing over through the ionomer membrane with hard GDLs or soft GDLs during the wet/dry cycle test. The initial H_2 crossover was negligibly small (ca. 0.01%) for both cells. The GDLs had significant impact on the wet/dry cycling durability of the membranes. With the hard GDLs, the H_2 crossover rapidly increased after ca. 4,000 cycles and exceeded 2% at 5,000 cycles, implying mechanical failure of the membrane. In contrast, change of the H_2 crossover was minor with the soft GDLs and was ca. 0.03% even after 30,000 cycles. Similar results were obtained in our previous research using SPK membrane[18], where the use of sub-gaskets and

soft GDLs was effective in preventing the swelling-shrinking of the sulfonated poly(arylene ether ketone) (SPK) membrane, resulting in a significant improvement in the wet/dry cycling durability. The wet/dry cycle durability of the SPP-QP membrane was superior compared to the SPK membrane (H_2 crossover of the SPK membrane was ca. 0.5% after 20,000 cycles with the soft GDLs). The results suggest that lack of ether bonds in the polymer main chain in the SPP-QP membrane was effective in improving the chemical and mechanical durability of the aromatic hydrocarbon ionomer membranes.

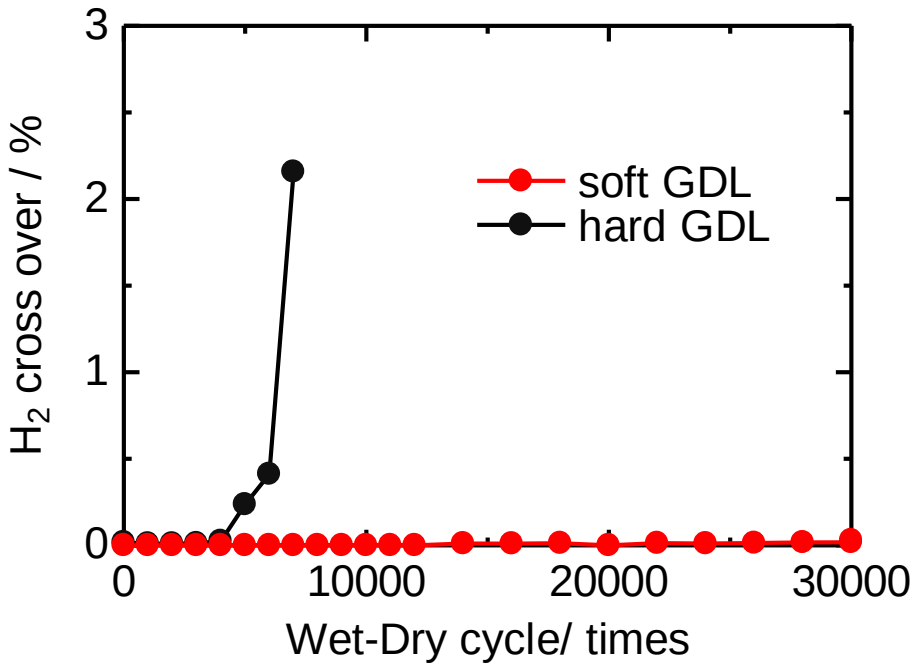

Figure 2-2 H_2 crossover during wet/dry cycle test

2.3.2 Post-test analyses of the MEAs. After the durability test, both cells were disassembled and the recovered MEAs were subjected to the He leak test. Figure 2-3 shows the amount of permeated He through the MEAs at 36 different locations. The MEA with the hard GDLs showed high He leakage (ca. 1.52×10^{-4} m^3 Pa s^{-1} on average). Significant He leak over the detection limit was observed at the edge of the catalyst layer (the boundary with the sub-gasket). Strain due to the swelling and shrinkage during the wet/dry cycle test occurred in the ionomer membrane, which caused mechanical failure, in particular, at the interface of the membrane and the catalyst layer under the gasket where the membrane was fixed and the dimensional change was restricted. The MEA with the soft GDLs exhibited much smaller He leakage (ca. 3.44×10^{-5} m^3 Pa/s on average). It is noted that the maximum He leakage was 6.56×10^{-5} m^3 Pa/s, 69% smaller than that with the hard GDLs at the same location. During the wet/dry cycles, stress was concentrated on the edges of the membrane where significant dimensional changes occurred with the hard GDL. The soft GDL, which was adhered to the catalyst layer, deformed in accordance with the membrane swelling and shrinkage, and mechanically held it to prevent the membrane rupture (Figure 2-4).The He leakage of the post-test SPP-QP membrane with the soft GDLs was even smaller than that of the post-test SPK membrane (ca. 1.0×10^{-4} m^3 Pa s^{-1} on average)[18], further supporting the above-mentioned idea on the better durability of the SPP-QP membrane.

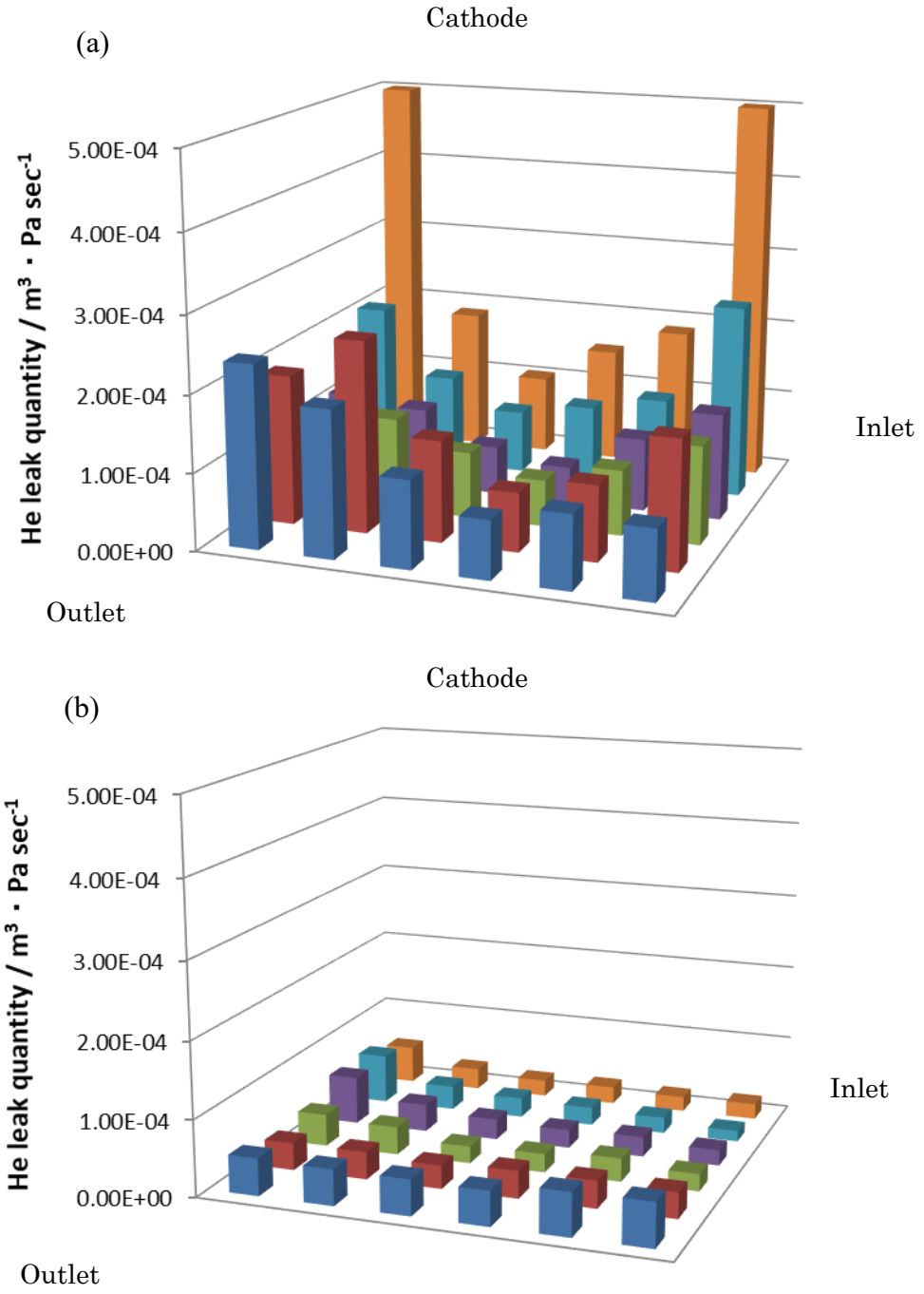

Figure 2-3 He leakage of the MEAs using (a) hard GDL and (b) soft GDL at 36 locations.

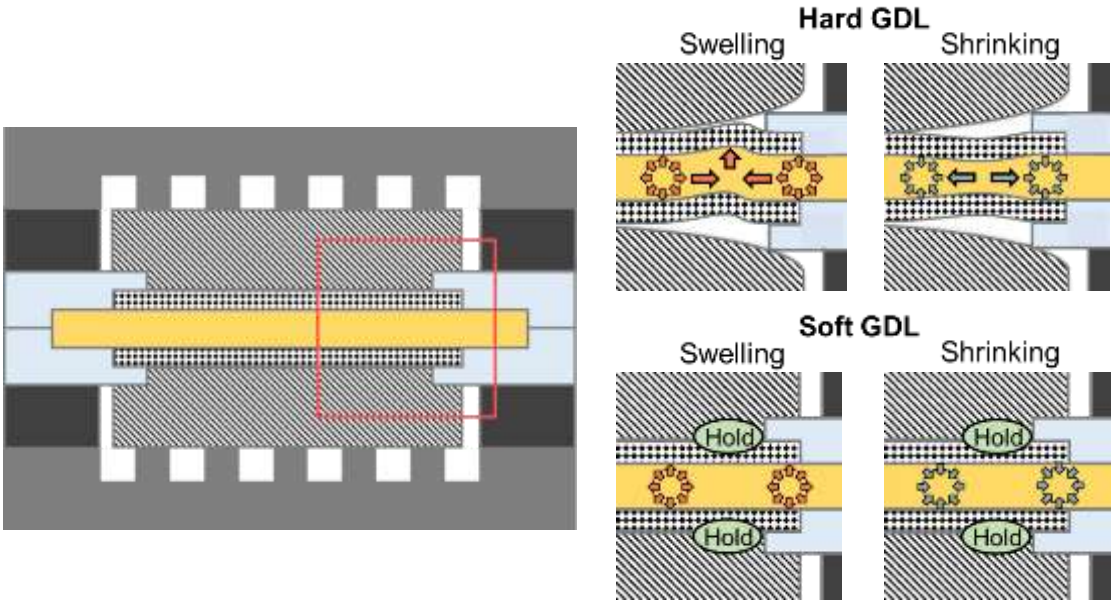

Figure 2-4 Schematic model of the MEAs at the edge of the catalyst layer with hard or soft GDLs.

2.3.3 Post-test analyses of the membranes. The catalyst layers were carefully removed from the MEAs, and the resulting post-test membranes were analyzed. Figure 2-5 shows the molecular weight distribution (gel permeation chromatography) curves of the post-test membrane at three different locations and the pristine membrane for reference. The molecular weight data are summarized in Table 2-2. The post-test membrane with the hard GDLs showed changes in the elution curves, in particular, under the sub-gasket for which the peak shifted to the lower molecular weight (M_p = 63.0 kDa) compared to the pristine membrane (M_p = 83.2 kDa). At the center and the edge of the membrane, a shoulder appeared

at the higher molecular weight (ca. 300 kDa) and a minor peak appeared at the lower molecular weight (ca. 3 kDa) while the main peak did not change. The higher molecular weight portion may suggest some ionic cross-linking with di- or trivalent metal cationic contaminants. The lower molecular weight portion may indicate minor polymer degradation, *e.g.*, loss of the sulfonic acid groups. As a result, the polydispersity (M_w/M_n) became larger. With the soft GDLs, the recovered membrane showed fewer changes in the GPC curves. The effect was the most striking under the sub-gasket, for which M_n, M_w, M_p and polydispersity values were similar to those of the pristine membrane. The results suggest that the soft GDLs were effective in mitigating both mechanical and chemical decomposition of the ionomer membranes. However, the shoulder and minor peak were also detected at the center and the edge of the post-test membrane with the soft GDLs in larger intensity than that with the hard GDLs, probably because of the larger number of wet/dry cycles (30,000) with the soft GDLs compared to that (7,000) with the hard GDLs.

(a)

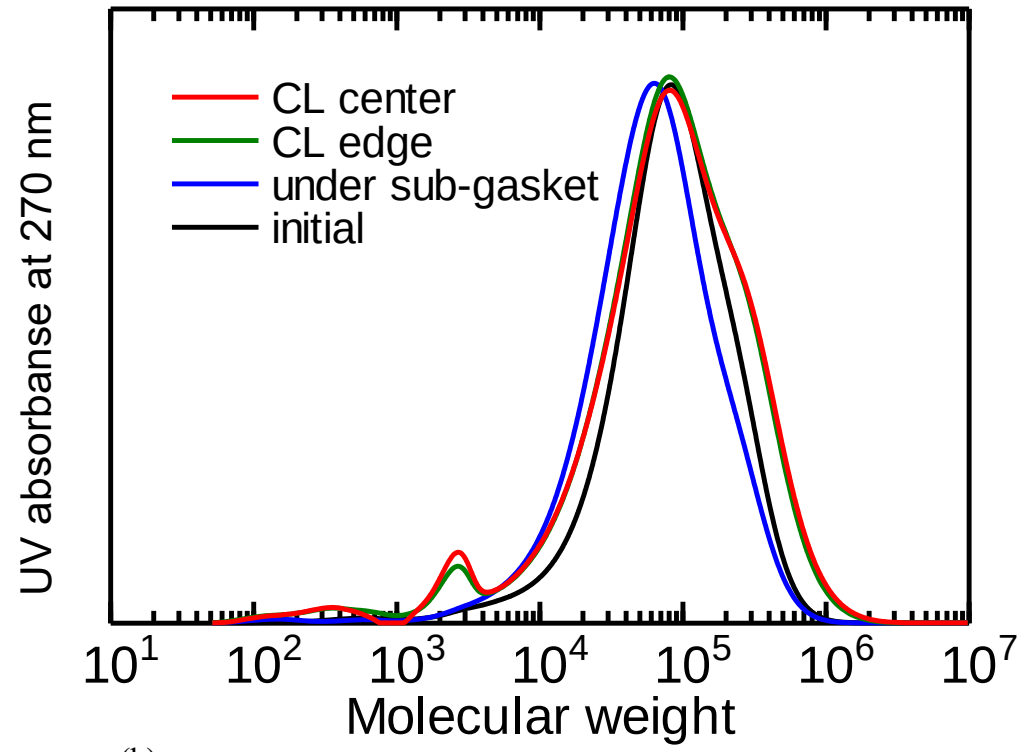

(b)

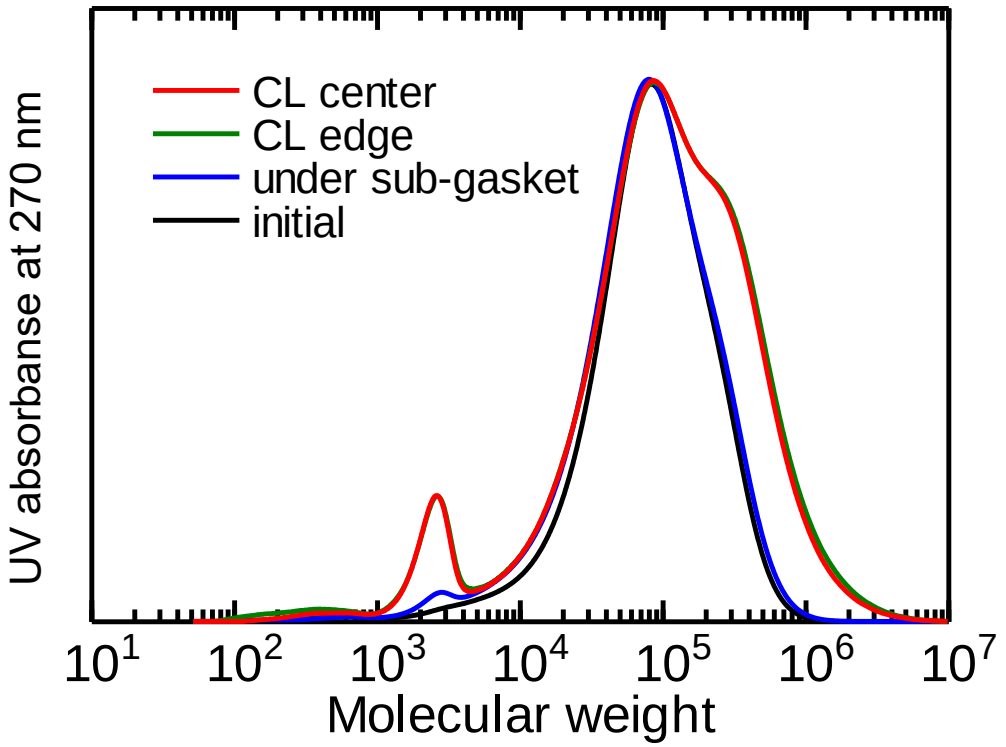

Figure 2-5 Molecular weight distribution curves of pristine and post-test SPP-QP membranes after the wet/dry cycling test (a) using the hard GDLs and (b) the soft GDLs.

Table 2-2 Molecular weight data of the SPP-QP membranes at different locations before and after the wet-dry cycling test using the hard and soft GDLs

		*M*n (kDa)	*M*w (kDa)	*M*p (kDa)	*M*w/*M*n
hard GDL	center	10.3	151	81.0	15
	edge	9.60	144	80.4	15
	under sub-gasket	17.5	94.0	63.0	5.4
soft GDL	center	17.3	218	86.1	13
	edge	11.9	228	86.1	19
	under sub-gasket	23.4	120	78.8	5.1
initial (pristine)		28.1	119	83.2	4.2

Figure 2-6 shows ^{1}H NMR spectra of the post-test membranes at three different locations (similar to the GPC analyses) and the pristine membrane. In both membranes, the NMR spectra of the samples at the center and the edge were in fair agreement with that of the pristine membrane. Close examination revealed that peak 5, assignable to the sulfophenylene protons, was slightly smaller in intensity at the center and under the sub-gasket. The copolymer composition and IEC values were calculated from the peak integrals and are summarized in Table 2-3 to confirm that the changes in the composition and the concentration of the sulfonic acid groups were minor at all locations. The results further support the chemical robustness of the SPP-QP membrane in wet/dry cycle testing for 30,000 cycles.

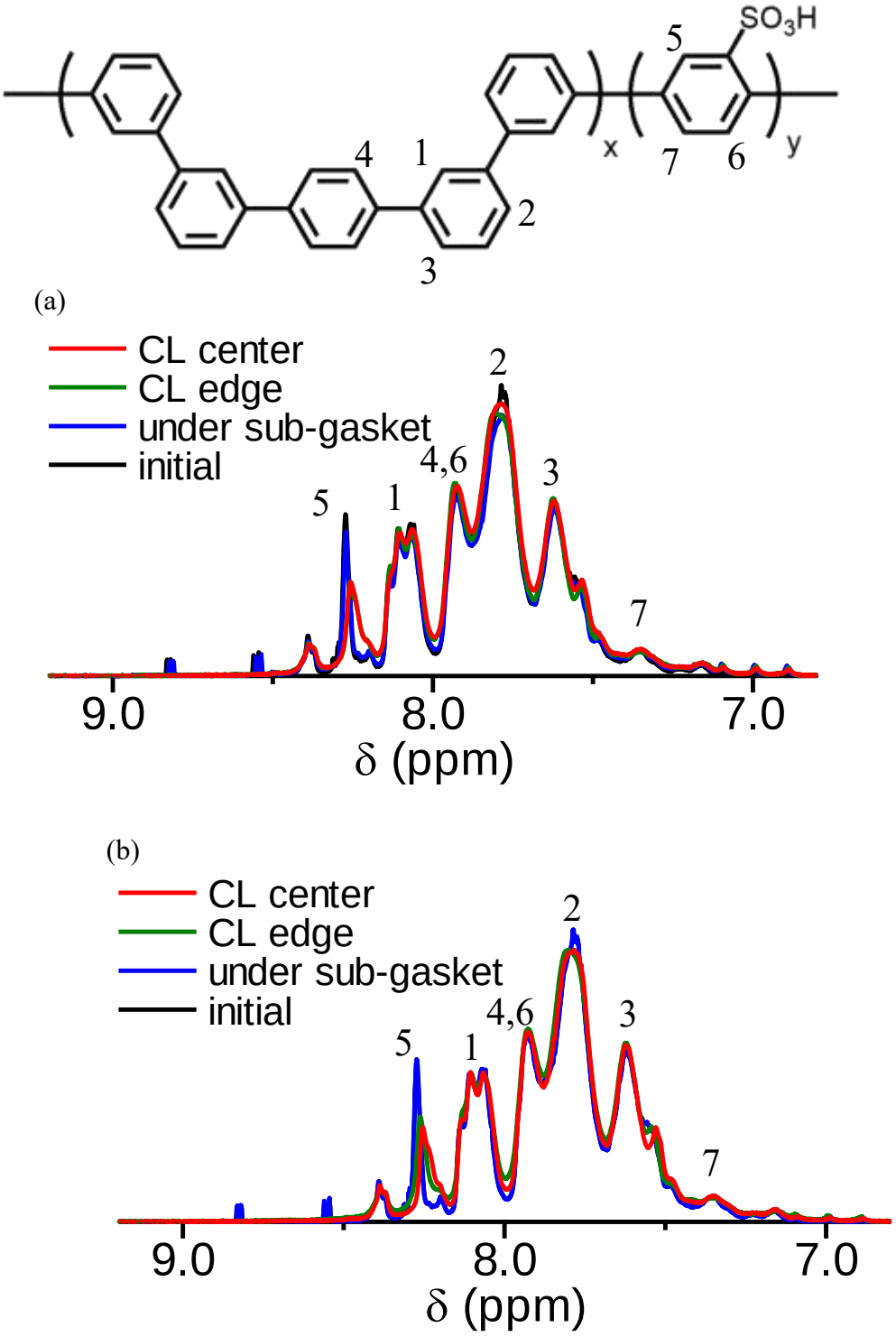

Figure 2-6 ^{1}H NMR spectra of SPP-QP membranes at different locations before and after the wet-dry cycling test (a) using the hard GDLs and (b) the soft GDLs.

Table 2-3 Copolymer composition and IEC of the SPP-QP membranes at different locations before and after the wet/dry cycling test using the hard and soft GDLs

		hydrophilic : hydrophobic (mol mol^{-1})	IEC (mequiv g^{-1})
hard GDL	center	35 : 65	2.80
	edge	34 : 66	2.86
	under sub-gasket	34 : 66	2.82
soft GDL	center	35 : 65	2.76
	edge	33 : 67	2.94
	under sub-gasket	34 : 66	2.83
initial (pristine)		34 : 66	2.87

Figure 2-7 shows stress-strain curves of the post-test membranes at three different locations, as well as the pristine membrane. The maximum strain of the post-test membranes was lower than that of the pristine membrane at all locations. In particular, the loss of the strain was severe at the edge and under the sub-gasket (the maximum strain was smaller than 20%). At the center, the degradation was not significant. Even with the soft GDL, the mechanical strength of the post-test membrane deteriorated because of the larger cycle numbers with the soft GDL (30,000 cycles) than the hard GDL (7,000 cycles), as discussed above. The results indicate that the SPP-QP membrane lost mechanical strength when the chemical structure was not changed. As we reported recently[20], a reinforcement strategy was effective and will be further investigated.

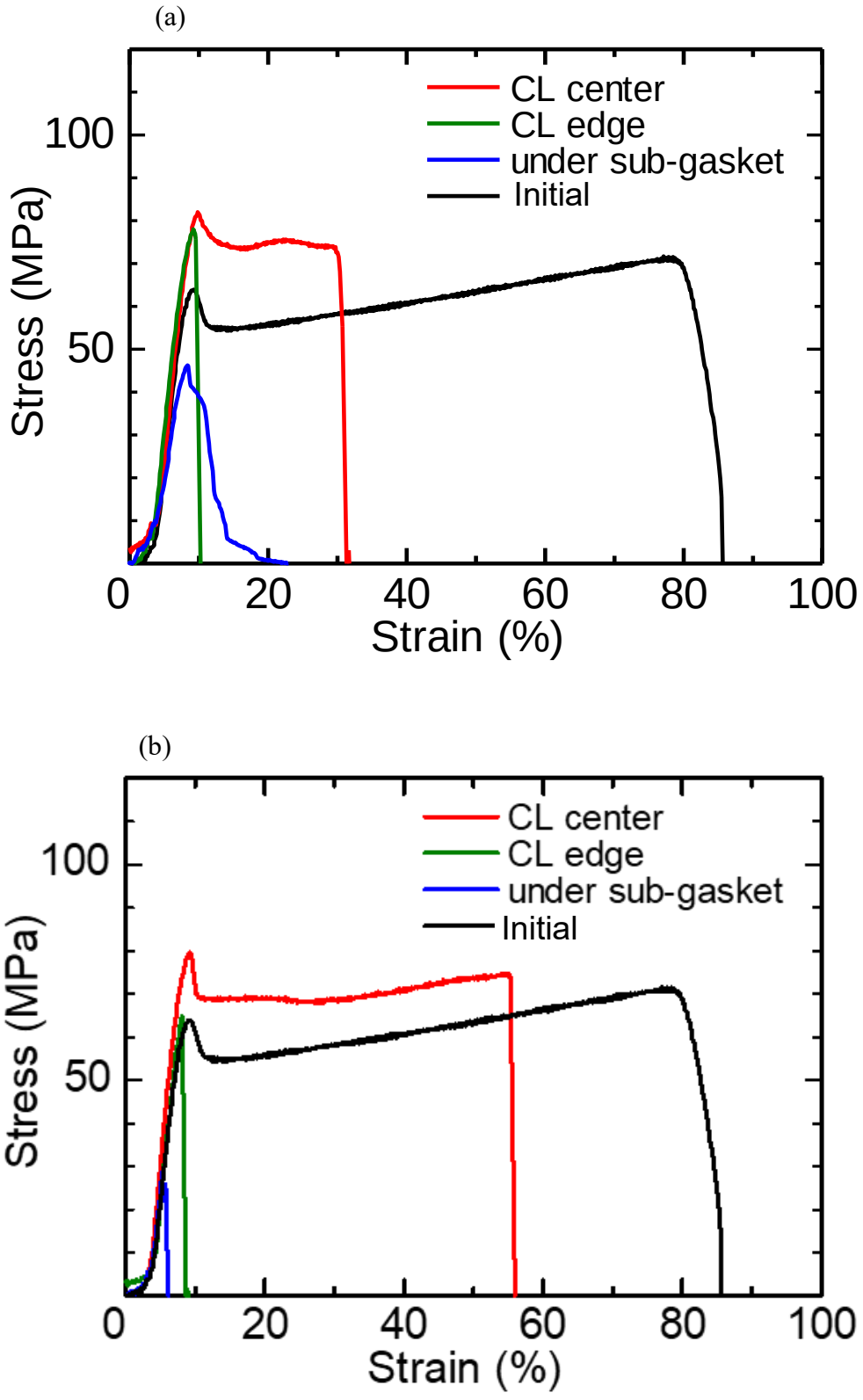

Figure 2-7 Stress-strain curves of pristine and post-test SPP-QP membranes after the wet/dry cycling test (a) using the hard GDLs and (b) the soft GDLs.

2.4 Conclusions

The mechanical durability of our sulfonated polyphenylene ionomer (SPP-QP) membranes was evaluated using different gas diffusion layers (hard GDLs or soft GDLs), where the SPP-QP swelled under humidified conditions and shrank under dry conditions. The membrane experienced mechanical failure at the interface with the catalyst layer under the gasket with the hard GDLs after 4,000 cycles. In contrast, the membrane was much more durable with the soft GDLs preventing the rupture of the membrane upon swelling/shrinking. The He leakage of the post-test membrane with the soft GDLs was ca. 3.44×10^{-5} m^3 Pa s^{-1} on average, and was much smaller than that with the hard GDLs (ca. 1.52×10^{-4} m^3 Pa s^{-1} on average). In addition to the mechanical degradation, the membrane showed only minor loss in the sulfonic acid groups and some possible cross-linking (via metal cationic contaminants), as suggested by the GPC and NMR analyses. SPP-QP membrane withstood 30,000 cycles in the wet/dry cycle test with the soft GDLs, similar to our previous hydrocarbon ionomer (SPK) membranes, whereas chemical degradation seemed less, due to its robust polymer structure having no heteroatom linkages in the main chain. The SPP-QP membrane, however, lost mechanical strength after the test, even with the soft GDL, which will be improved by physical reinforcement with porous materials.

2.5 References

1. L. Carrette, K. A. Friedrich, U. Stimming, *fuel cells*, 1 (2001) 5-39.
2. J. Meurig Thomas, P. P. Edwards, P. J. Dobson, G. P. Owen, *Journal of Energy Chemistry*, **51** (2020) 405-415.
3. H.A. Gasteiger, S.S. Kocha, B. Sompalli, F.T. Wagner, *Appl., Catal.B*, **56** (2005) 9-35.
4. M. Watanabe, D. A. Tryk, M. Wakisaka, H. Yano, H. Uchida, *Electrochim. Acta,* **84** (2012) 187-201.
5. L. Osmieri, J. Park, D. A. Cullen, P. Zelenay, D. J. Myers, K. C. Neyerlin, *Curr. Opin. in Electrochem.*, **25** (2021) 100627.
6. H. Zhang, P.K. Shen, *Chem. Rev.* **112** (2012) 2780-2832.
7. M.P. Rodgers, L. J. Bonville, H. R. Kunz, D. K. Slattery, J. M. Fenton, *Chem. Rev.*, **112** (2012) 6075-6103.
8. W. Liu, T. Suzuki, H. Mao and T. Schmiedel, *J. Electrochem. Soc*. **50** (2013) 51-64.
9. Y. Prykhodko, K. Fatyeyeva, L. Hespel, S. Marais, *Chem. Eng. J.*, **409** (2021) 127329.
10. C.H. Park, C.H. Lee, M.D. Guiver, Y.M. Lee, *Prog. Polym. Sci.*, **36** (2011) 1443-1498.
11. J. Miyake, T. Mochizuki, K. Miyatake, *ACS Macro Lett*. **4** (2015) 750-754.
12. T.J.G. Skalski, M. Adamski, B. Britton, E. M. Schibli, T.J. Peckham, T. Weissbach, T. Mochizuki, S. Lyonnard, B.J. Frisken, S. Holdcroft, *ChemSusChem*., **11** (2018) 4033−4043.

13. Peressin, N. Adamski, M. Schibli, E. M. Ye, E. Frisken, B. J. Holdcroft, *S. Macromolecules*, **53** (2020) 3119−3138.

14. G. H. Byun, J. A. Kim, N. Y. Kim, Y. S. Cho, C. R. Park, *Mater. Today. Energy*, **17** (2020) 100483.

15. Sutradhar, S. C. Rahman, M. M. Ahmed, F. Ryu, T. Lei, J. Yoon, S. Lee, S. Jin, Y. Kim, *W. J. Power Sources*, **442** (2019) 227233.

16. V.A. Sethuraman, J.W. Weidner, A.T. Haug, L.V. Protsailo, *J. Electrochem. Soc.* **155** (2008) B119-B124.

17. H. Ishikawa, Y. Fujita, J. Tsuji, M. Kusakabe, J. Miyake, Y. Sugawara, K. Miyatake and M. Uchida, *J. Electrochem. Soc.*, **164** (2017) F1204-F1210.

18. H. Ishikawa, T. Teramoto, Y. Ueyama, Y. Sugawara,Y. Sakiyama, M. Kusakabe, K. Miyatake, M. Uchida, *J. Power Sources*, **325** (2016) 35-41.

19. J. Miyake, R. Taki, T. Mochizuki, R. Shimizu, R. Akiyama, M. Uchida, K. Miyatake, *sci. Adv*., **3** (2017) 0476.

20. J. Miyake, T. Watanabe, H. Shintani, Y. Sugawara, M. Uchida, and K. Miyatake, *ACS Mater. Au*, **1** (2021) in press.

21. DOE cell component accelerated stress test protocols for PEM fuel cells, 2007 (accessed 22.5.16),

https://www1.eere.energy.gov/hydrogenandfuelcells/fuelcells/pdfs/component_durabil

ity_profile.pdf.

Chapter 3 Aromatic ionomer in the anode catalyst layer Improves start-up durability of polymer electrolyte fuel cells

3.1 Introduction

To improve performance and durability and reduce costs, significant efforts have been devoted to the development of component materials, including electrocatalysts and electrolyte membranes. [1-4]Proton-conductive ionomers are used as binders in the catalyst layers and are thus particularly important in terms of how they affect the electrocatalytic activity for the oxygen reduction and hydrogen oxidation reactions (ORR and HOR) in operating PEFCs. Currently, perfluorinated ionomers such as Nafion are most used in commercial PEFCs due to their high proton conductivity and chemical stability. However, the fully fluorinated chemical structure leads to high production costs. Their glass transition temperature is relatively low (ca. 100 - 110 ºC) and becomes even lower under hydrated conditions, which limits the upper operable temperature of PEFCs, whereas the US -DOE and the New Energy and Industrial Technology Development Organization (NEDO) of Japan both target an operating temperature of 120 ºC within the next decade. Therefore, there is a strong demand for proton-conductive ionomers with higher thermal stability and lower production cost.[5-7] Aromatic ionomers are some of the more promising candidates and have been extensively investigated. For example, sulfonated poly(phenylene)s,[8, 9] poly(ether ether ketone)s[10], poly(arylene ether sulfone)s[11] and polyimides[12] can be found as proton-exchange

membranes in the literature, and some of these have been applied as electrode binders.[13-19] Recently, E. Balogun et al. reported high fuel cell performance above 1 W cm^{-2}.using their original polyphenylene ionomer.[20] We have developed polyphenylene ionomer (SPP-QP) membranes, which consist only of phenylene rings and sulfonic acid groups. Unlike typical aromatic ionomers, the absence of heteroatoms in groups such as ethers and sulfones in the polymer main chain contributed to excellent chemical stability, in addition to high proton conductivity over a wide humidity range, comparable to that of Nafion. High fuel cell performance and durability have been achieved with the SPP-QP membrane in cells in which Nafion was used in the catalyst layers.[21] As a next step, it is of great interest to investigate the properties of SPP-QP as an electrode binder. In the present study, SPP-QP was evaluated as the catalyst layer binder for both the anode and cathode. It is well-known that the carbon support in the cathode catalyst layer corrodes during the cell start-up, most likely due to the high cathode potential (> 1.5 V vs RHE) due to the reverse current reaction caused by the ORR in the anode (Figure 1).[22,23] In the literature, there have been several attempts to address this issue, including the use of more corrosion-resistant catalysts and support materials in the cathode.[24,25] I report herein that strong “specific” adsorption of SPP-QP on the platinum surface suppressed the reduction of oxygen remaining in the anode as a reverse current reaction, and thus that it mitigated the degradation of the cathode catalyst layers in the accelerated durability test (or gas exchange durability test) simulating start-up conditions.

Post-test analyses of the catalyst layers and fuel cell performance were carried out to support this claim.

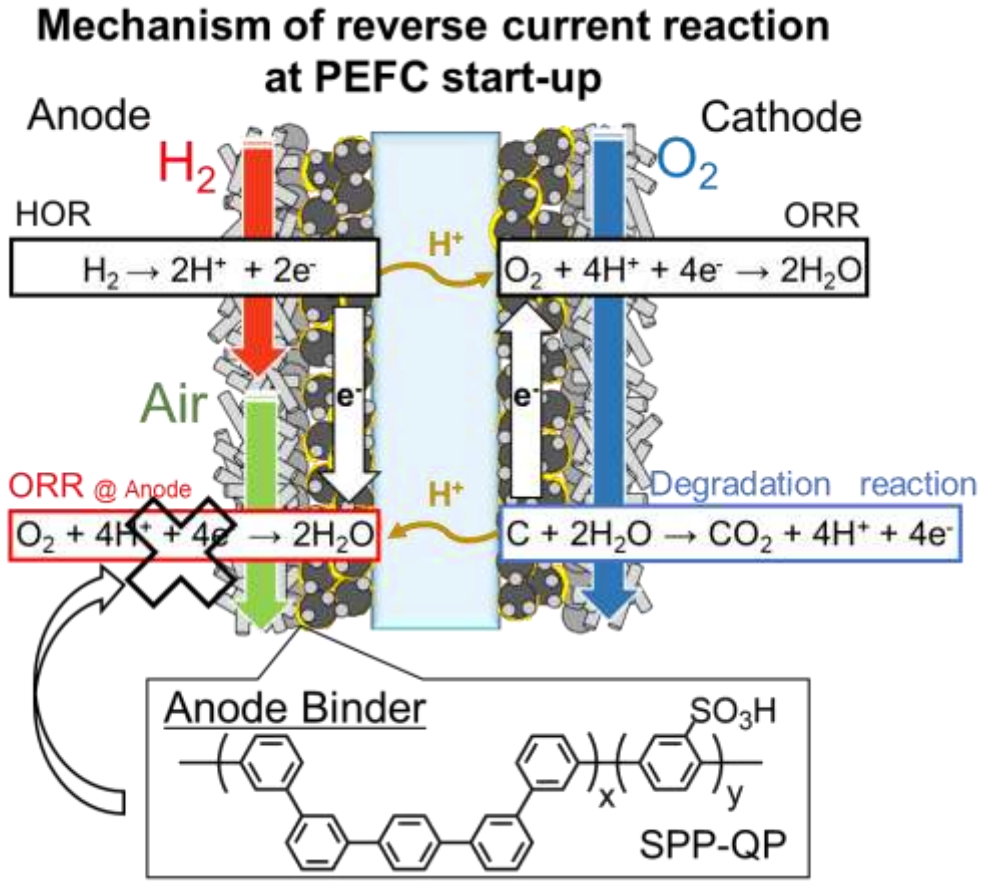

Figure 3-1 Mechanism of reverse current reaction during start-up of a PEFC.

3.2 Experimental

3.2.1 Preparation of membrane electrode assembly (MEA)

The SPP-QP (IEC = 2.4 mequiv g^{-1}) ionomer was synthesized according to the literature. A 5-wt% ionomer solution in dimethylacetamide (DMAc) was filtered through a 1-μm disk filter prior to use. Nafion solution (IEC = 0.95 ~ 1.03 mequiv g^{-1}, D-521) was purchased from Dupont. A catalyst ink containing SPP-QP was prepared from the ionomer solution, Pt/CB (TEC10E50E, Tanaka Kikinzoku Kogyo, K. K.), ultrapure water, and DMAc. A catalyst ink containing Nafion was prepared from the ionomer solution, Pt/CB (TEC10E50E, Tanaka Kikinzoku Kogyo, K. K.), ultrapure water, and ethanol. In both inks, the mass ratio of the ionomer to carbon (I/C) and solid/liquid ratio were set at 0.7 and 0.07 wt%, respectively. The mixture was ball-milled in a zirconia pod containing 20 5-mm zirconia beads at 270 rpm for 30 min. The resulting ink was sprayed onto one side of a Nafion membrane (NRE211, Dupont) using the pulse-swirl-spray technique (PSS, Nordson). Then, the catalyst ink was similarly sprayed onto the other side of the membrane to obtain a catalyst-coated membrane (CCM). The geometric electrode area was 29.16 cm^2 and the Pt loading was 0.50 ± 0.05 mg cm^{-2}. The CCM was dried at 60 ºC overnight. The CCM was hot-pressed at 140 °C and 10 kgf cm^{-2} for 3 min and then sandwiched by two gas diffusion layers (29BC, SGL Carbon Group) and assembled into a JARI cell (Japan Automobile Research Institute).

3.2.2 Initial activation and cleaning of the cell

The single cell was placed in a fuel cell evaluation system (Panasonic Co.). For all cells with the catalyst layer containing SPP-QP or Nafion, initial activation[26] was carried out supplying oxygen to the SPP-QP electrode and hydrogen to the Nafion electrode at 80 °C and 100% RH at a constant current density of 0.2 A cm^{-2} for 12 h. Then, hydrogen was supplied to the anode and nitrogen (100 ml min^{-1}) was supplied to the cathode, respectively, and the potential was swept between 0.075 and 1.0 V at a sweep rate of 20 mV s^{-1} for 40 cycles. For the cell with the catalyst layer containing SPP-QP, nitrogen was exchanged to oxygen and the cell was operated at a constant current density of 1.0 A cm^{-2} for 48 h to remove the residual DMAc solvent from the catalyst layer.

3.2.3 Fuel cell operation

The cell was operated at 80 ºC and 100% RH. Cyclic voltammograms (CV) were obtained with a potential sweep between 0.075 and 1.0 V at a sweep rate of 20 mV s^{-1} with 100 ml min^{-1} of hydrogen supply at the anode and nitrogen atmosphere in the cathode. From the obtained hydrogen adsorption peak and the Pt oxidation peak in the CV, the electrochemically active surface area (ECSA) and Pt oxidation charge (Q_{Pt}) were calculated, respectively. The Q_{Pt} was calculated from the anodic charge in the CV between 0.7 - 0.85 V subtracting the electric double layer charge (around 0.4 V) as the baseline. The polarization curves were measured at a constant current mode with hydrogen supplied to the anode and

oxygen supplied to the cathode. The gas utilization percentages were 70% for hydrogen and 40% for oxygen. Polarization at the anode was measured by a hydrogen pump test[22] under each measurement condition supplying hydrogen at 1 L min^{-1}.

3.2.4 Accelerated durability test

Gas exchange durability test was conducted at 45 ºC with the protocol shown in Table 1.[27] The degradation of the cathode catalyst was monitored by measuring CV every 200 cycles at 45 ºC and 100%RH.

Table 1 Protocol for gas exchange durability test

		anode			cathode		
step	time (s)	gas	RH (%)	flow rate mL min^{-1}	gas	RH (%)	flow rate mL min^{-1}
1	90	Air	0	360	Air	100	360
2	90	H_2	100	38	Air	100	360
3	60	N_2	0	180	N_2	0	180

3.2.5 FIB-SIM

After the durability test, the recovered MEA was disassembled, sliced by a focused ion beam and analyzed by scanning ion microscopy (FIB-SIM, FB-2200, Hitachi High-Technologies Co., Ltd.).

3.3 Results and Discussion

3.3.1 Evaluation of the cell using SPP-QP as the cathode

Figure 3-2 shows cyclic voltammograms of the cells using SPP-QP and Nafion as the cathode binder (hereinafter referred to as the SPP-QP(c)-cell and Nafion(c)-cell, respectively) at 80 ºC. The CVs differed between the two cells, in particular, in the high potential region (0.6 - 1.0 V vs. RHE). At 100% RH, SPP-QP (c)-cell showed a characteristic peak around 0.2 V assignable to adsorption/desorption of the sulfonic acid groups in addition to the hydrogen adsorption/desorption. ECSA values calculated from the hydrogen adsorption peaks were 45.1 $m^2\ g^{-1}$ for SPP-QP(c)-cell and 44.4 $m^2\ g^{-1}$ for Nafion(c)-cell, respectively, suggesting that the ionomers in both cathode catalyst layers functioned similarly as proton sources for the catalysts. In contrast, the Pt oxidation peak shifted to higher potentials for the SPP-QP(c)-cell than for the Nafion(c)-cell. The Q_{Pt} value calculated from the Pt oxidation peak (0.7 - 0.85 V) was 29.1 C g^{-1} for the SPP-QP(c)-cell, which was nearly exactly half than that (62.5 C g^{-1}) for the Nafion(c)-cell. These results indicate that

SPP-QP was more strongly adsorbed on the Pt catalyst and thus suppressed the surface oxidation by excluding water in the double layer, although its bulk water absorbability was larger. The differences in the Q_{Pt} values became even larger at lower humidity (53% RH, Table 2), further supporting this idea, since, at lower humidity, the ionomer concentration became higher and there was less water available.

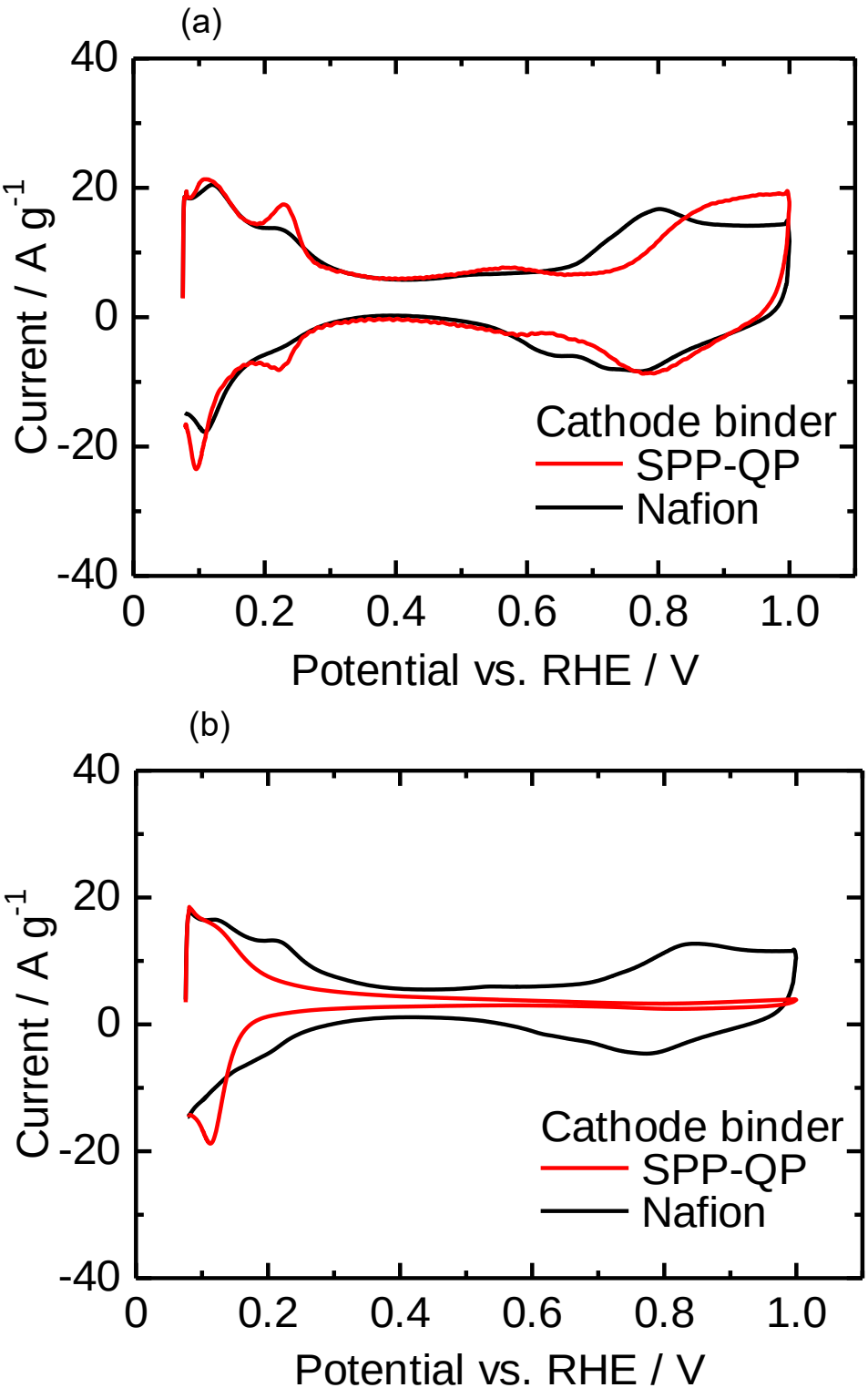

Figure 3-2 Cyclic voltammograms for the cathodes of the SPP-QP(c)-cell and Nafion(c)-cell at 80 ºC: (a) 100% RH and (b) 53% RH.

Table 2 ECSA and Q_{Pt} values for the cathodes of the SPP-QP(c)-cell and Nafion(c)-cell.

	100% RH		53% RH	
	ECSA (m^2 g^{-1})	Q_{Pt} (C g^{-1})	ECSA (m^2 g^{-1})	Q_{Pt} (C g^{-1})
SPP-QP(c)-cell	45.1 ±0.3	29.1 ± 4.1	29.8 ±4.0	0
Nafion(c)-cell	44.4 ±0.2	62.5 ±3.7	35.0 ±1.1	37.0 ±3.1

Figure 3-3a shows I-V curves and ohmic resistance of the SPP-QP(c)-cell or Nafion(c)-cell at 80 ºC and 100% RH. The ohmic resistances were comparable and constant for both cells (ca. 0.05 Ω cm^2) and reasonable for the proton conductivity and thickness of the Nafion membrane, indicating that the interfacial contact between the membrane and the catalyst layers containing the Nafion and SPP-QP binders was excellent. The performance of the SPP-QP(c)-cell was lower than that of Nafion(c)-cell. From the *IR*-corrected I-V curves (Figure 3-4), the lower performance was due to the larger cathodic overpotential. The mass activity (MA) of the Pt catalyst at 0.85 V was 42.8 A g^{-1} for the SPP-QP(c)-cell, which was ca. 21% that for the Nafion(c)-cell (201 A g^{-1}). The fuel cell performance became even lower at 53% RH (Figure 3-3b), resulting in a lower MA, 18.8 A g^{-1}, for the SPP-QP(c)-cell compared to 147 A g^{-1} for the Nafion(c)-cell. The results are in good accordance with the CV curves, as mentioned above, where the specific absorption of the SPP-QP binder on the Pt surface became stronger at lower humidity and at higher potential.

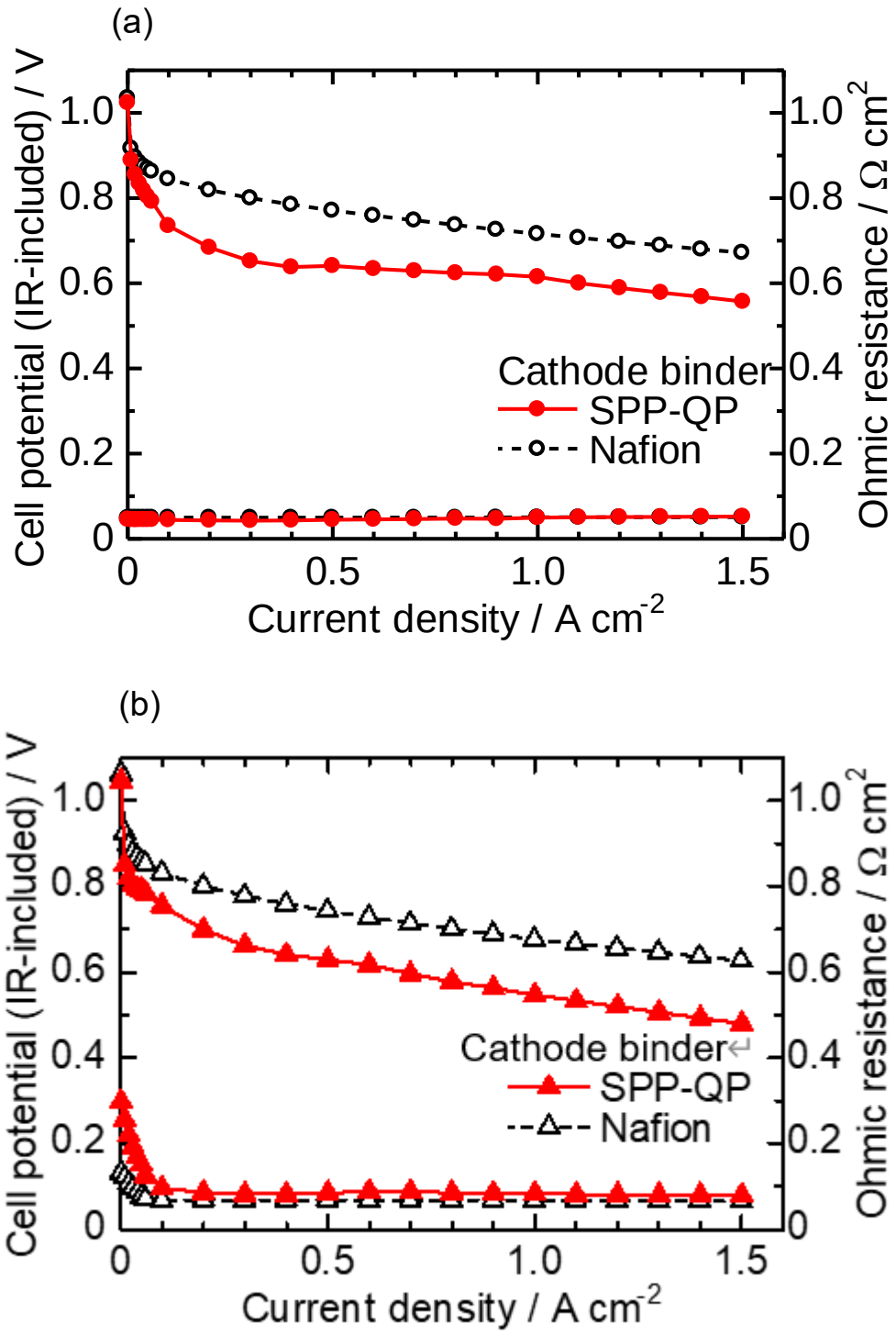

Figure 3-3 I-V curves (IR-included) and ohmic resistances for the SPP-QP(c)-cell and Nafion(c)-cell at 80 ºC: (a) 100% RH and (b) 53% RH.

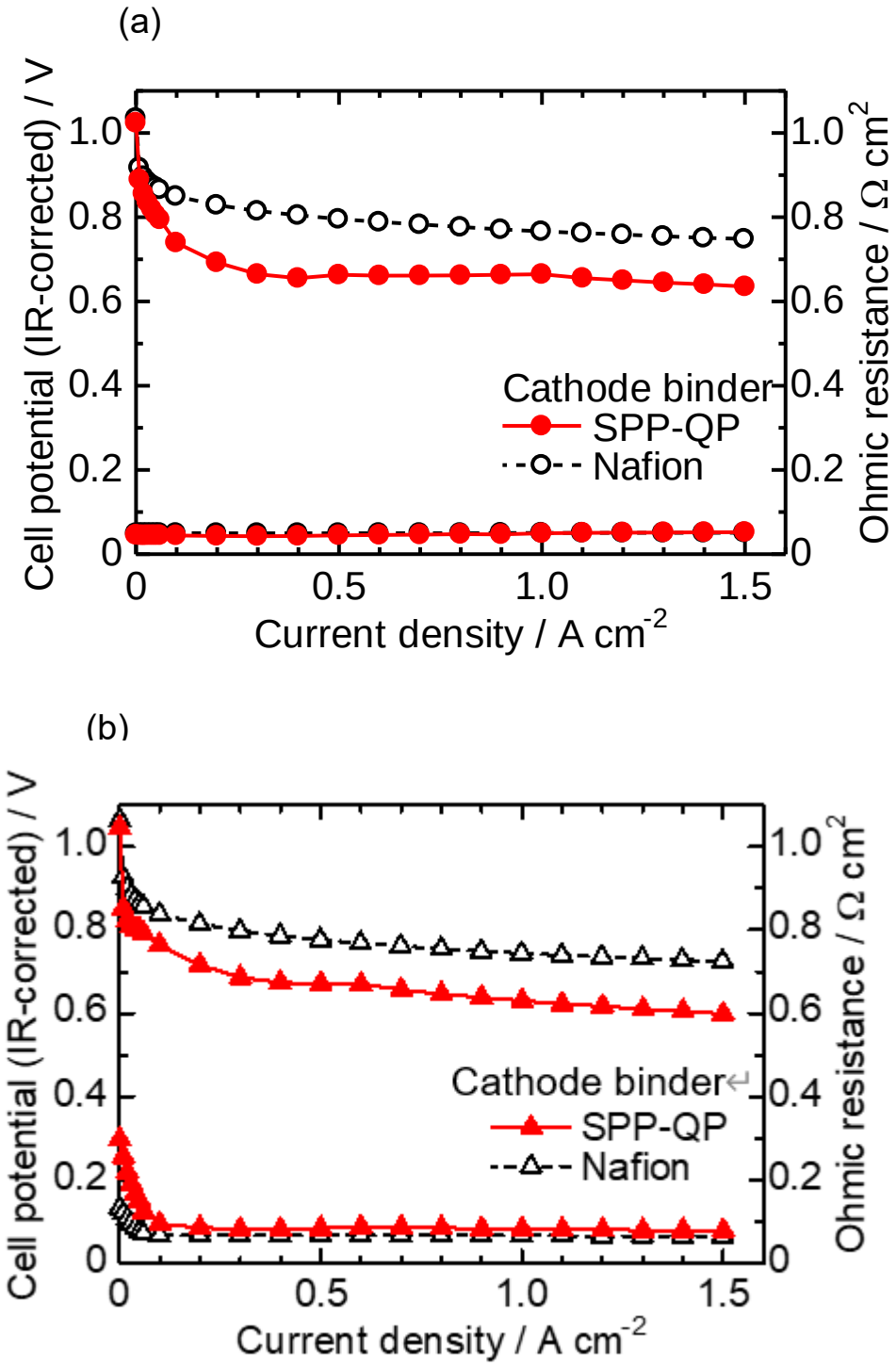

Figure 3-4 I-V curve (IR-corrected) and ohmic resistance of the SPP-QP(c)-cell and Nafion(c)-cell at 80 ºC; (a) 100% RH and (b) 53% RH.

3.3.2 Initial performance of the cell using SPP-QP as the anode binder

Figure 3-5 shows the anodic polarization of a cell using SPP-QP and Nafion as the anode binder (hereinafter referred to as the SPP-QP(a)-cell and Nafion(a)-cell, respectively) at 80 ºC, 100% RH and 53% RH (note that cathode binder was Nafion for both cells). At 100% RH, the anodic polarization was negligibly small at current densities up to 1.5 A cm^{-2} for both cells. At 53% RH, the polarization was somewhat larger, 50 mV for the Nafion(a)-cell and 81 mV for the SPP-QP(a)-cell at the current density of 0.9 A cm^{-2} due to the lower proton conductivity of the binders. The anodic polarizations were much smaller than the cathodic polarizations (Figure 3-3) at 80 ºC 100% RH and 53% RH, implying that SPP-QP as well as Nafion functioned well as the proton conductor for the HOR.

Figure 3-6 shows I-V curves and ohmic resistances of the SPP-QP(a)-cell and Nafion(a)-cell at 80 ºC (a) 100% RH, (b) 53% RH. The ohmic resistances were similar to those of the SPP-QP(c)-cell and Nafion(c)-cell in Figure 3-3, indicating reasonable compatibility of the SPP-QP-based anode catalyst layer and Nafion membrane. The SPP-QP(a)-cell showed slightly lower cell performance than the Nafion(a)-cell (*e.g.*, lower by 49 mV at 100% RH and 50 mV at 53% RH at a current density of 0.15 A cm^{-2}), where the cathode performance was responsible (Figure 3-7). In order to achieve complete removal of the residual solvent from the SPP-QP binder, a stringent cleaning process was applied to the SPP-QP(a) cell (see the Experimental Section) which might have caused such differences in the cathode performance.

Since the performance difference was rather minor, both cells were subjected to the durability test.

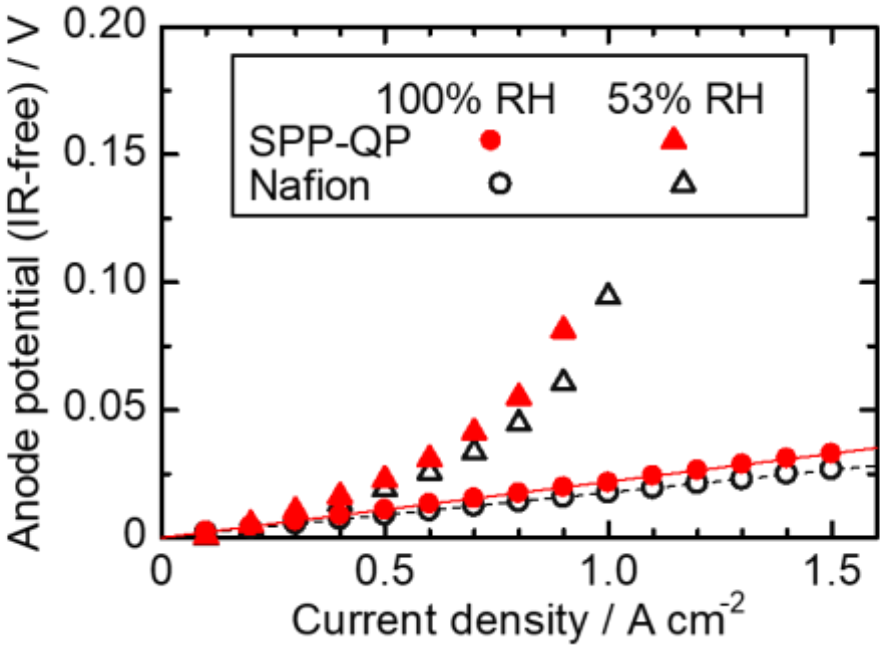

Figure 3-5 Anodic polarization for the SPP-QP(a)-cell and Nafion(a)-cell at 80 ºC.

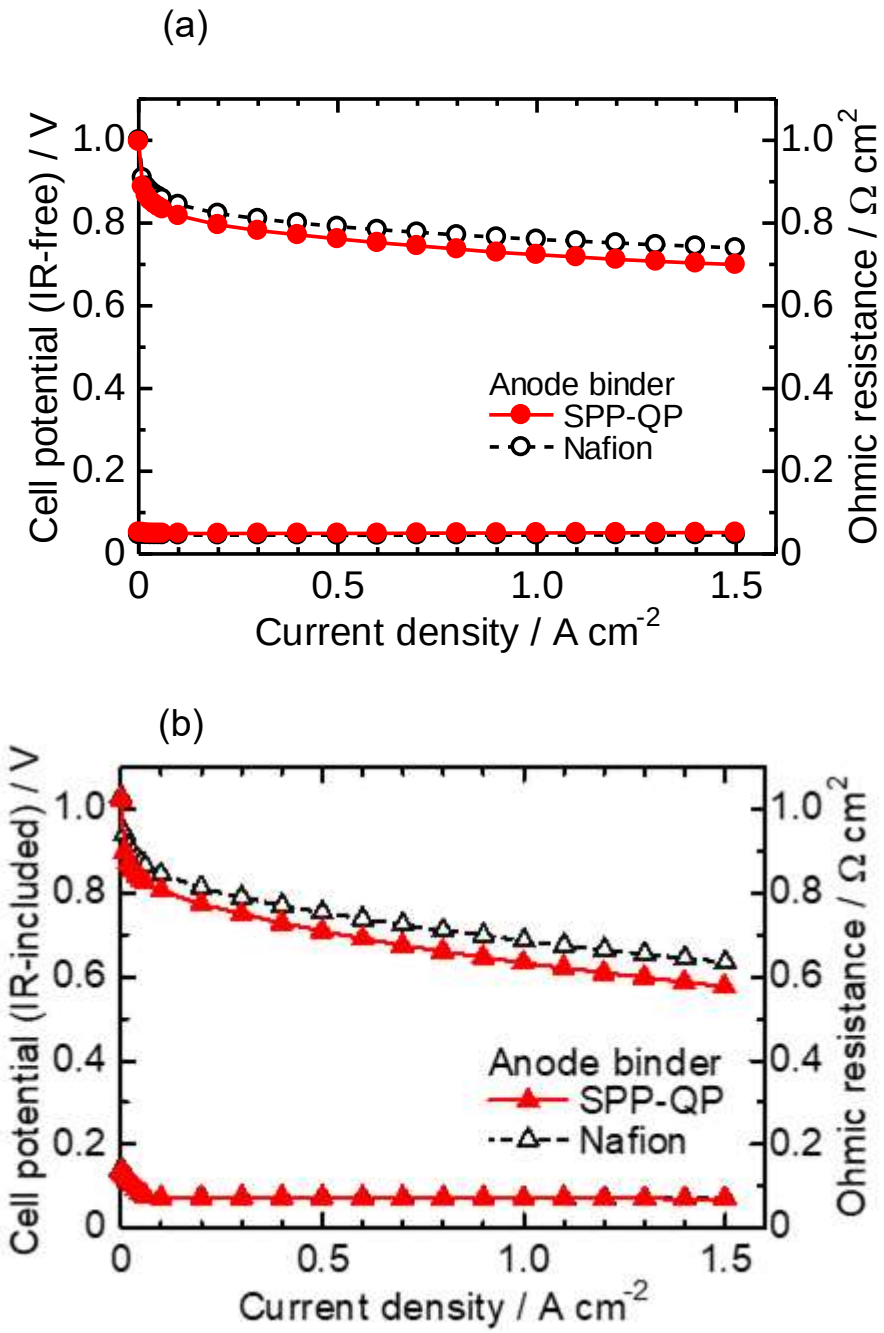

Figure 3-6 Polarization curves (IR-included) and ohmic resistances for the SPP-QP(a)-cell and Nafion(a)-cell at 80 ºC: (a) 100% RH and (b) 53% RH.

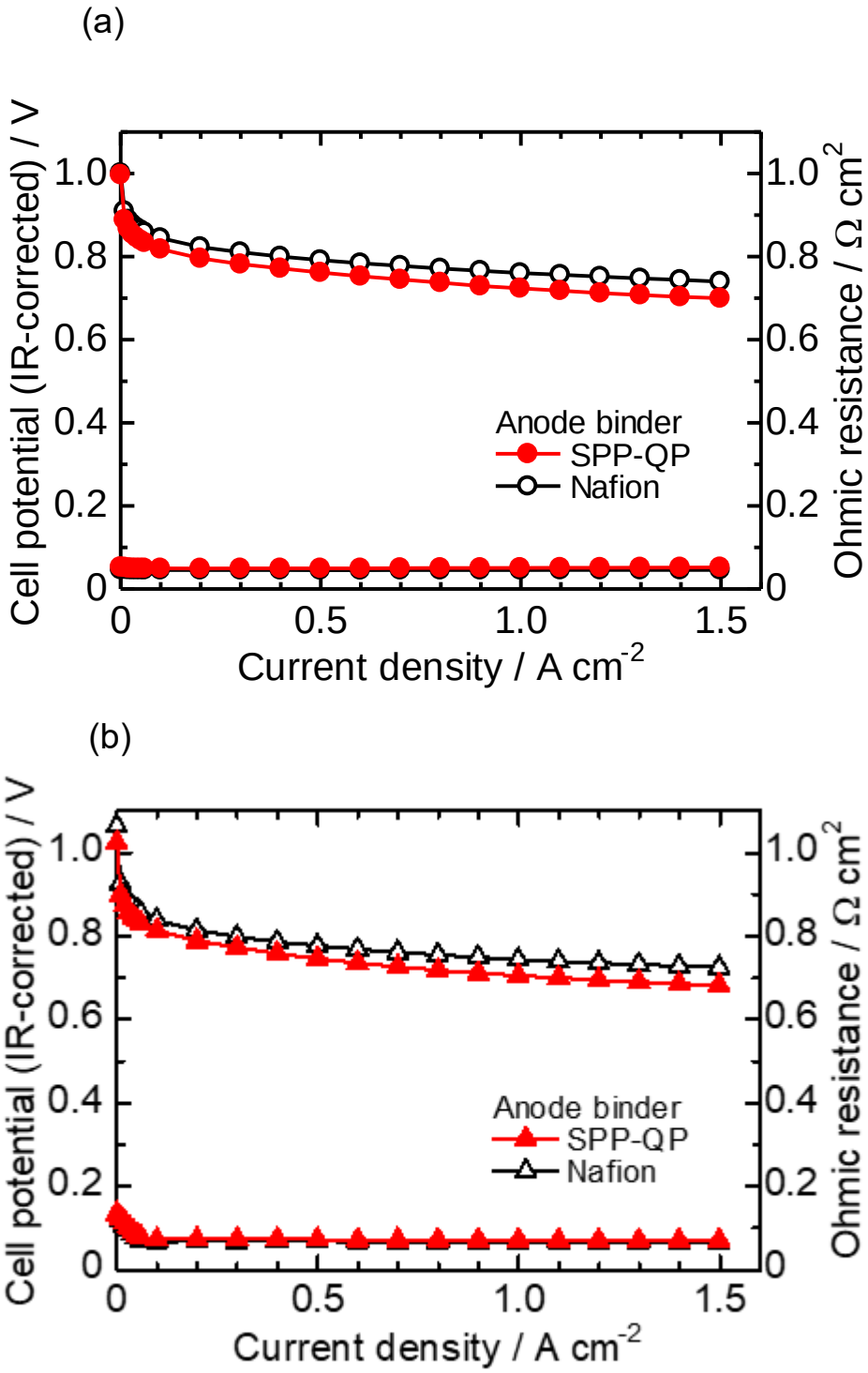

Figure 3-7 Polarization curve (IR-corrected) and ohmic resistance of the SPP-QP(a)-cell and Nafion(a)-cell at 80 ºC; (a) 100% RH and (b) 53% RH.

3.3.3 Accelerated durability test simulating fuel cell start-up

The durability of the cathodes of the SPP-QP(a)-cell and Nafion(a)-cell was examined via a gas exchange cycle test under accelerated conditions. Degradation of the cathode catalyst layers was monitored electrochemically via CVs obtained every 200 cycles. Figure 3-8 shows the changes in the CVs during the gas exchange cycle test[29]. In both cells, the current density based on hydrogen adsorption/desorption (from 0.075 to 0.4 V), electric double layer (from 0.4 to 0.7 V), and surface Pt oxidation/reduction (from 0.7 to 1.0 V) decreased with increasing cycle number. The results show that the gas exchange cycles induced the reverse current reaction, causing deterioration of the carbon support and loss of the Pt in the cathode catalyst layers. In order to monitor this process, ECSA and its retention calculated therefrom are plotted as a function of cycle number in Figure 3-9. The initial ECA for the SPP-QP(a)-cell was 48.1 $m^2 g^{-1}$, smaller than that for the Nafion(a)-cell (56.9 $m^2 g^{-1}$). Although the initial ECA was lower, the decay was smaller for the SPP-QP(a)-cell, retaining a higher ECSA (17.9 $m^2 g^{-1}$, 37% retention) than that (10.5 $m^2 g^{-1}$, 19% retention) for the Nafion(a)-cell after 1000 cycles. The average decay of the ECSA was 0.03 $m^2 g^{-1}$ cycle (or 0.45 $m^2 g^{-1}$ h) and 0.05 $m^2 g^{-1}$ cycle (or 0.70 $m^2 g^{-1}$ h) for the SPP-QP(a)-cell and Nafion(a)-cell, respectively. The superior durability of the ECSA in the cathode of the SPP-QP(a)-cell was due to the stronger specific adsorption of SPP-QP on the Pt catalyst at higher potentials, as discussed above. The ORR occurring at the anode (under start-up conditions) was suppressed,

mitigating the reverse current reaction, increase of the cathode potential, and, accordingly, corrosion of the carbon support in the cathode catalyst layer.[20]

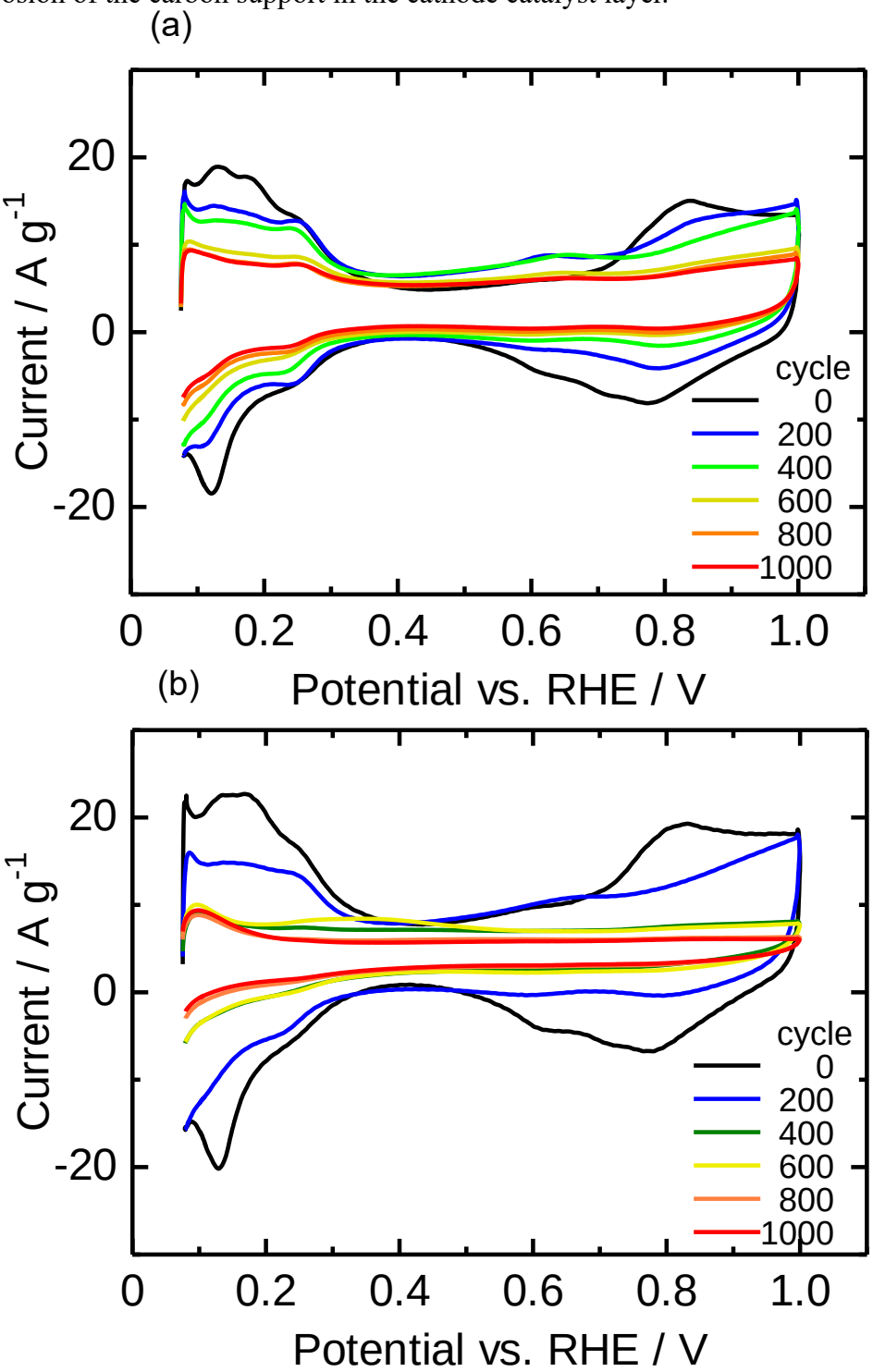

Figure 3-8 CVs for the cathode of the (a) SPP-QP(a)-cell and (b) Nafion(a)-cell during the gas exchange cycle test.

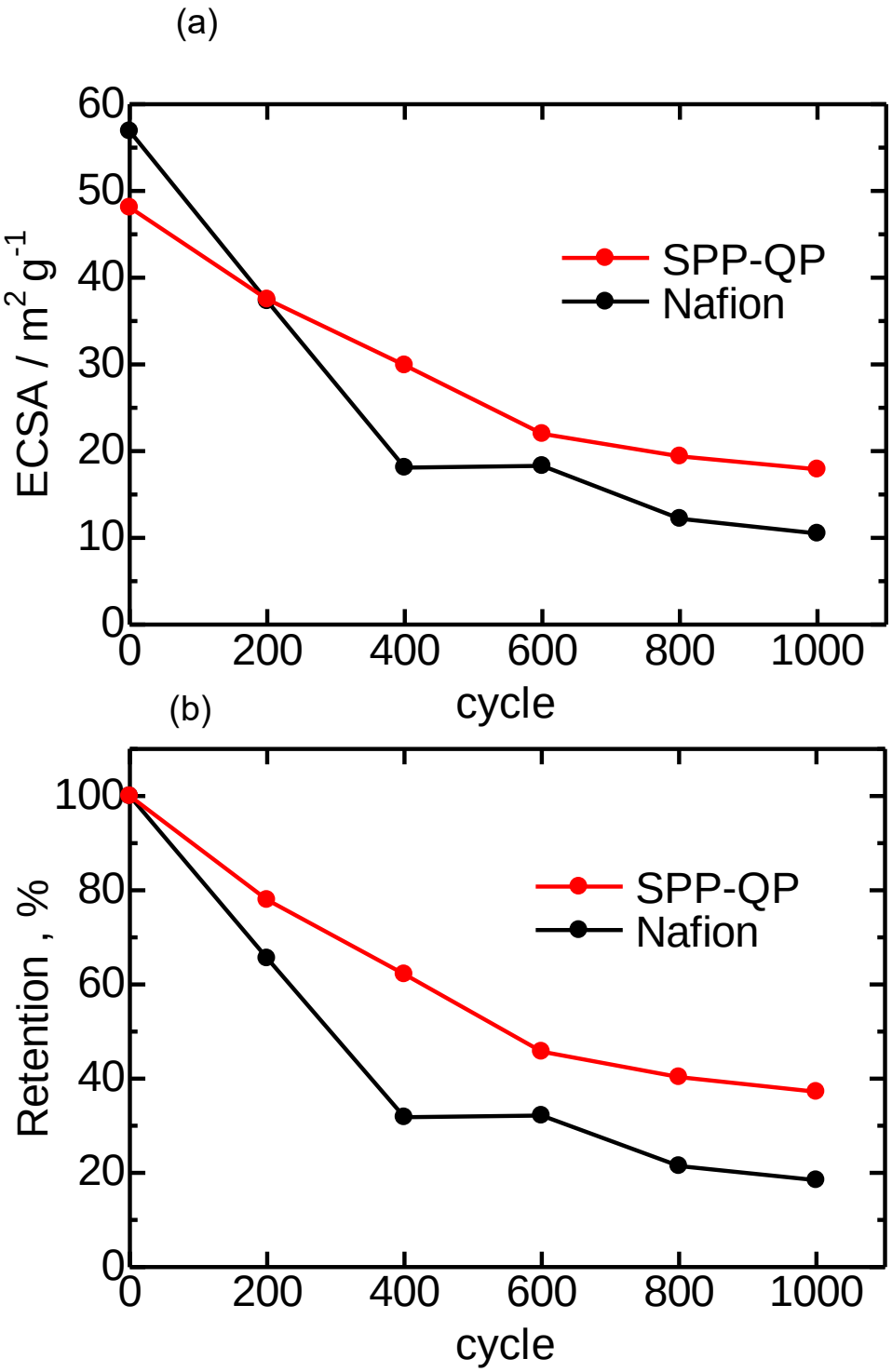

Figure 3-9 (a) ECSA and (b) ESCA retention for the SPP-QP(a)-cell and Nafion(a)-cell during the gas exchange cycle test.

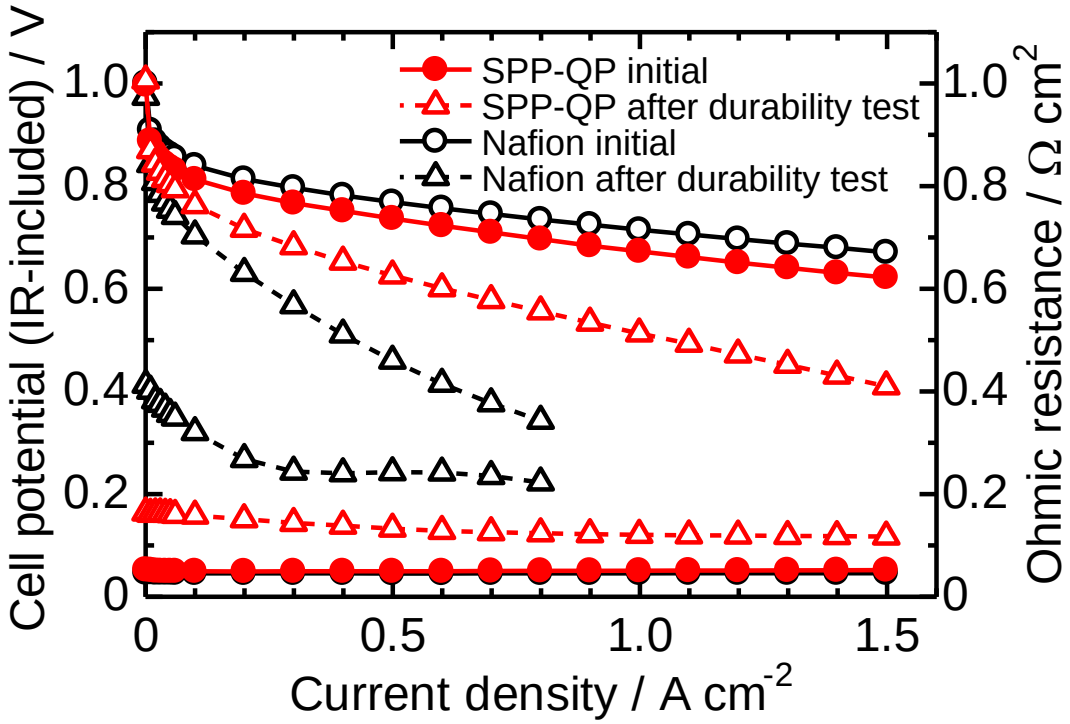

Figure 3-10 IR-included polarization curve and ohmic resistance of the SPP-QP(a)-cell and Nafion(a)-cell before and after the gas exchange cycle test at 80 ºC and 100% RH.

After 1000 cycles, the I-V curves and ohmic resistance were re-evaluated and compared with the initial performance (Figure 3-10). Both cells exhibited lower I-V performance and higher ohmic resistance after the test due to the degradation of the cathode catalyst layers. The performance loss was less significant for the SPP-QP(a)-cell than for the Nafion(a)-cell. For example, the cell voltages measured at a current density of 0.8 A cm^{-2} were 0.56 V (80% of the initial) for the SPP-QP(a)-cell and 0.34 V (47% of the initial) for the Nafion(a)-cell. These results are consistent with the ECSA losses mentioned above. This result means that the specific adsorption of SPP-QP to Pt suppressed the ORR at the anode, which triggers the

deterioration reaction at PEFC startup. Although the initial ohmic resistance was very similar (ca. 0.05 Ω cm^{-2}) for both the SPP-QP(a)-cell and Nafion(a)-cell, the post-test ohmic resistance differed: 0.12 Ω cm^{-2} for the SPP-QP(a)-cell and 0.22 Ω cm^{-2} for the Nafion(a)-cell. The carbon carrier of the cathode catalyst layer deteriorated by the gas replacement durability test and the contact resistance increased, and the influence was larger in the Nafion (a) cell.

3.3.4 Post-test analyses of the cathode catalyst layers

Figure 3-11 compares cross-sectional scanning ion microscopic (SIM) images of the cathode catalyst layers at three different locations of the cells before and after the 1000-cycle gas exchange test (SIM was used rather than SEM to obtain more distinct contrast in the images). The thickness of the catalyst layers was initially ca. 17 μm. After the test, the thickness was smaller than 6 μm at the inlet, center, and outlet for the Nafion(a)-cell. These results were indicative of the significant degradation of the cathode catalyst layers associated with the carbon corrosion. In contrast, the SPP-QP(a) cell retained its original thickness, specifically at the inlet (17 μm). However, even for the SPP-QP (a)-cell, the catalyst layer became thinner at the center and the outlet, probably because of the longer time period during which the mixed gas remained downstream.

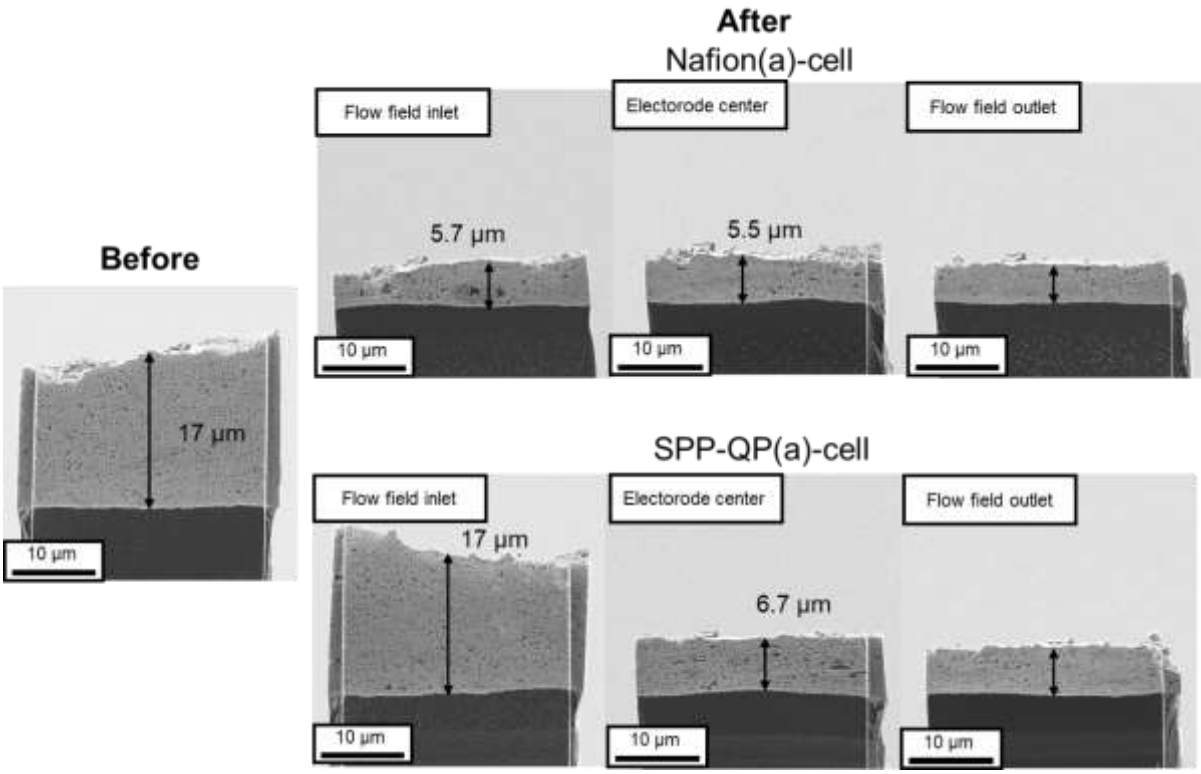

Figure 3-11 SIM images of the cathode catalyst layer of the SPP-QP(a)-cell and Nafion(a)-cell before and after the gas exchange cycle test.

3.4 Conclusions

Our in-house sulfonated polyphenylene ionomer (SPP-QP) was evaluated as a catalyst layer binder for the anode and the cathode, in separate measurements. From the CVs, the cell using SPP-QP as the cathode binder (SPP-QP(c)-cell) exhibited an ECSA value comparable with that for the cell using Nafion as the cathode binder (Nafion(c)-cell) at high (100% RH) and low (53% RH) humidity, indicating that SPP-QP functioned well as a proton conductor in the catalyst layer. However, the Pt oxidation peak for the SPP-QP(c)-cell shifted to higher potentials, and the Q_{Pt} value was half that of the Nafion(c)-cell because of the strong specific adsorption of the SPP-QP ionomer on the Pt catalyst, particularly at low humidity. Therefore, the SPP-QP(c)-cell exhibited lower fuel cell performance than that for the Nafion(c)-cell. At 53% RH, the difference in mass activity (MA) of the cathode catalyst was ca. 7.8-fold. As the anode binder, SPP-QP functioned well in a fuel cell (SPP-QP(a)-cell), with negligibly small anodic overpotential and only slightly inferior I-V performance compared to the Nafion(a)-cell, even at 53% RH. The specific adsorption of SPP-QP on Pt at higher potentials contributed much to improving the durability of the cathode catalyst layer during the start-up (or gas exchange) durability test. The cathode ECSA values remaining for the SPP-QP(a)-cell and Nafion(a)-cell after 1000 cycles were 17.9 $m^2\ g^{-1}$ (37% remaining) and 10.5 $m^2\ g^{-1}$ (19% remaining). In other words, the reverse current reaction was suppressed under start-up conditions with the SPP-QP as the anode binder. The post-test I-V performance was such

that the cell voltages measured at a current density of 0.8 A cm^{-2} were 0.56 V (80% remaining) for the SPP-QP(a)-cell and 0.34 V (47% remaining) for the Nafion(a)-cell. The ohmic resistance after the test was lower for the SPP-QP(a)-cell (0.12 Ω cm^{-2}) than for the Nafion(a)-cell (0.22 Ω cm^{-2}). In the Nafion(a)-cell, the interfacial compatibility between the Nafion membrane and the cathode catalyst layer deteriorated due to the degradation of the cathode catalyst layer. In the Nafion(a)-cell, the cathode catalyst layer became thinner than 6 μm in all areas (initial thickness 17 μm). In contrast, the SPP-QP(a)-cell retained the initial thickness of the cathode catalyst layer, specifically at the inlet (16 μm). I have thus, demonstrated that the use of aromatic ionomer as the anode binder, which exhibited strong specific adsorption on Pt, was effective in mitigating the cathode carbon corrosion during a gas exchange test simulating start-up conditions, with little or no impact on the I-V performance.

3.5 References

1. H.A. Gasteiger, S.S. Kocha, B. Sompalli and F.T. Wagner, *Appl. Catal. B-Enyiron.*, **56**, (2005), 9-35.
2. M. Watanabe, D. A. Tryk, M. Wakisaka, H. Yano and H. Uchida, *Electrochim. Acta*, **84,** (2012), 187-201.
3. L. Osmieri, J. Park, D. A. Cullen, P. Zelenay, D. J. Myers and K. C. Neyerlin, *Curr. Opin. Electrochem.*, **25,** (2021), 100627.
4. H. Zhang and P. K. Shen, *Chem. Rev*. **112,** (2012), 2780-2832.
5. M. P. Rodgers, L. J. Bonville, H. R. Kunz, D. K. Slattery and J. M. Fenton, *Chem. Rev.*, **112,** (2012), 6075-6103.
6. W. Liu, T. Suzuki, H. Mao and T. Schmiedel, *J. Electrochem. Soc.* **50,** (2013), 51-64.
7. Y. Prykhodko, K. Fatyeyeva, L. Hespel and S. Marais, *Chem. Eng. J.*, **409,** (2021), 127329.
8. M. Adamski, N. Peressin and S. Holdcroft, *Mater. Adv.*, **2**, (2021), 4966-5005.
9. T. Oshima, M. Yoshizawa-Fujita, Y. Takeoka, and M. Rikukawa, *ACS Omega*, **1**, (2016), 939–942.
10. J. Jiang, X. Zhu, H. Qian, J. Xu, Z. Yue, Z. Zou and H. Yang, *Sustainable Energy & Fuels* **3**, (2019), 2426−2434.
11. R. Mukherjee, A. K. Mandal and S. Banerjee, *e-Polymers,* **20**, *(*2020), 430−442.

12. A. G. Kumar, A. Singh, H. Komber, B. Voit, B. R. Tiwari, M. T. Noori, M. M. Ghangrekar and S. Banerjee, *ACS Appl. Mater. Interfaces*, **10**, (2018), 14803−14817.

13. T. Yoda, T. Shimura, B. Bae, K. Miyatake, M. Uchida, H. Uchida and M. Watanabe, *Electrochim. Acta*, **54**, (2009), 4328-4333.

14. T. Yoda, T. Shimura, B. Bae, K. Miyatake, M. Uchida, H. Uchida and M. Watanabe, *Electrochim. Acta,* **55**, (2010), 3464-3470.

15. T. Omata, M. Uchida, H. Uchida, M. Watanabe and K. Miyatake, *Phys. Chem. Chem. Phys*., **14**, (2012), 16713–16718.

16. T. Omata, M. Tanaka, K. Miyatake, M. Uchida, H. Uchida and M. Watanabe, *ACS Appl. Mater. Interfaces* **4**, (2012), 730−737.

17. H. Nguyen, F. Lombeck, C. Schwarz, P. A. Heizmann, M. Adamski, H. F. Lee, B. Britton, S. Holdcroft, S.Vierrath and M. Breitwieser, *Sustainable Energy & Fuels,* **5**, (2021), 3687-3699.

18. J. E. Chae, S. J. Yoo, J. Y. Kim, J. H. Jang, S. Y. Lee, K. H. Song and H. Kim, *Int. J. Hydrogen Energy,* **45,** (2020), 32856-32864.

19. X. Pu, Y. Duan, J. Li, C. Ru and C. Zhao, *J. Power Sources*, **493**, (2021), 229671.

20. E. Balogun, M. Adamski and S. Holdcroft, *J. Electrochem. Soc.,* **167**, (2020), 084502.

21. J. Miyake, R. Taki, T. Mochizuki, R. Shimizu, R. Akiyama, M. Uchida and K. Miyatake, *Sci. Adv.*, **3**, (2017), eaao0476.

22. C. A. Reiser, L. Bregoli, T. W. Patterson, J. S. Yi, J. Deliang, M. L. Perry and T. D. Jarvi, *Electrochem. Solid-State Lett.*, **8**, (2005), A273.

23. L. Dubau, L. Castanheira, F. Maillard, M. Chatenet, O. Lottin, G. Maranzana, J. Dillet, A. Lamibrac, J. Perrin, E. Moukheiber, A. Elkaddouri, G. D. Moor, C. Bas, L. Flandin and N. Caque, *WIREs Energy Environ.*, **3**, (2014), 540-560.

24. H. Shintani, Y. Kojima, K. Kakinuma, M. Watanabe and M. Uchida, *J. Power Sources*, **294**, (2015), 292–298.

25. Y. Yamashita, S. Itami, J. Takano, K. Kakinuma, H. Uchida, M. Watanabe, A. Iiyama, and M. Uchida, *J. Electrochem. Soc.*, **164**, (2017), F181-F187.

26. Fuel Cell Commercialization Conference of Japan, http://fccj.jp/pdf/23_01_kt.pdf.

27. Y. Yamashita, S. Itami, J. Takano, M. Kodama, K. Kakinuma, M. Hara, M. Watanabe, and M. Uchida, *J. Electrochem. Soc.*, **163**, (2016), F644-F650.

Chapter 4 General Conclusion and Future Prospect

4.1 General Conclusion

The realization of a new social system centered on hydrogen is extremely important for solving the energy problems currently facing the world. Although PEFCs, which are the core devices of the product, have begun to spread, further improvement in performance and durability is required for widespread use in the global market. Electrolyte membranes and catalysts in the constituent materials are very important in terms of performance and durability. In Chapter 2, the mechanical durability of our hydrocarbon polymer electrolyte membrane, poly(sulfophenylene quinquephenylene) (SPP-QP) or polyphenylene ionomer, was evaluated in wet/dry cycle tests in fuel cells according to the US-DOE protocol, where the effect of gas diffusion layers (hard or soft GDL) was investigated. The membrane exhibited mechanical failure with the hard GDL and H_2 crossover (permeation through the membrane) jumped from 0.01% to ca. 2% after 4,000 cycles. Post-test analyses indicated that the edge of the membrane under the gasket was the most damaged, where the dimensional change upon humidification/dehumidification was restricted. Use of the soft GDL significantly improved the wet/dry cycle durability of the membrane with no practical changes in the H_2 crossover, even after 30,000 cycles, due to the strong adhesion of the GDL to the catalyst layers. The mechanical durability of the SPP-QP membrane was better than that of our previous aromatic-based ionomer membrane containing ether and ketone groups

in the main chain. The loss of molecular weight and the sulfonic acid groups was rather minor for the SPP-QP membrane, indicating the chemical robustness of the membrane under the severe wet/dry cycle conditions. In Chapter 3, SPP-QP was used as a catalyst layer binder in polymer electrolyte fuel cells. SPP-QP functioned well in the proton-conducting thin layers to show high electrochemically active surface area (ECSA) for the Pt catalysts. When used as the cathode binder, however, specific adsorption of SPP-QP on the Pt catalyst lowered the oxygen reduction reaction (ORR) activity, resulting in lower fuel cell performance compared to that using Nafion binder. In contrast, SPP-QP supported the hydrogen oxidation reaction (HOR) in the anode, with a negligibly small overpotential, similar to that for Nafion. Furthermore, the fuel cell with SPP-QP as the anode binder (SPP-QP(a)-cell) exhibited improved durability in a gas exchange cycle test simulating start-up conditions (according to the protocol suggested by the Fuel Cell Commercialization Conference of Japan). After 1000 cycles, the remaining ECSA was 37% for SPP-QP(a)-cell, compared to 19% for the Nafion(a)-cell. The better durability was further demonstrated in the I-V curves, where the cell voltage remaining at a current density of 0.8 A cm^{-2} was 80% of the pre-test value for the SPP-QP(a)-cell compared to 47% for the Nafion(a)-cell. The specific adsorption of SPP-QP on the Pt catalyst suppressed the unfavorable ORR in the anode and accordingly the so-called reverse current reaction under start-up conditions, mitigating the degradation of the cathode catalyst layer.

4.2 Future Prospects

Electrolyte membranes: SPP-QP membranes without heteroatom bonds are claimed to be very chemically stable comparable to perfluorinated electrolyte membranes, however, mechanical durability was still an issue. Experiments using the soft GDL of this study revealed the importance of the constituent materials which also significantly influenced the durability of the electrolyte membrane. This finding can be applied to other HC electrolyte membranes. Other possible approaches include reinforcement with more mechanically but non-proton conductive porous materials, such as ePTFE[1,] and modification of the molecular structure (such as long side chains). Commercial PTFEs employ perfluorinated ionomer membranes reinforced with porous ePTFE. If these studies proceed and mechanical stability improves comparable to that of the perfluorinated electrolyte membrane, the HC electrolyte membrane would stand more promising as an alternative material.

Electrolyte binder: It was shown that the use of HC electrolyte as an anode binder suppressed the reverse current reaction and improved the durability of the cathode catalyst layers at the time of starting PEFCs. On the other hand, when it was used as the cathode binder, there remains a problem that the ORR activity was lowered due to the specific adsorption with the Pt catalyst at low humidity and excessive swelling at high humidity. In order to solve this problem, it is effective to change the structure of the electrolyte. For

example, bending of the main chain, steric hindrance based on the pendant structure, and/or reduction of electron density in the aromatic rings with electron-withdrawing substituents. An example of my research is shown below. Two electrolytes with similar structures shown in Figure 4-2 were used as the cathode binder. From the Pt oxidation quantity (Q_{Pt}) calculated from the CV in Fig. 4-3 and ECA, the Q_{Pt} / ECA of SPP-BAF with fluorine showed a higher value than that of SPP-BPP. It was suggested that the inclusion of fluorine in the molecular structure is related to the interaction between the binder and Pt. From Figure 4-4 (a), the SPP-BAF cell showed superior performance over the SPP-BPP cell at all current densities. The specific activity of SPP-BAF calculated from the polarization curve @ 0.85V was about twice that of SPP-BPP. This result means that the decrease in ORR activity due to the HC binder was suppressed. Figure 4-5 shows the optimized molecular structure and calculated electron density distribution by density functional theory (DFT). The electron density of the aromatic ring of SPP-BAF is lower than that of SPP-BPP. This result suggests that fluorine, which is an electron-withdrawing group, reduced the electron density of the aromatic ring. Therefore, the introduction of fluorine into the HC electrolyte structure is one approach to suppressing the interaction between the HC binder and Pt.

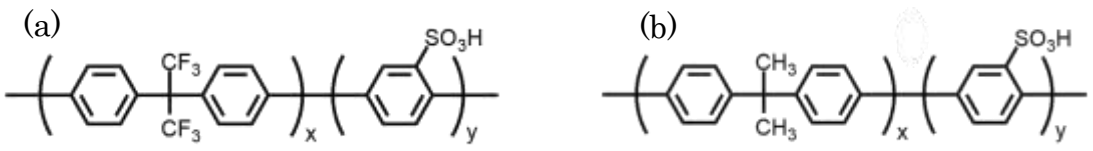

Figure 4-2 Molecular structure of cathode binder (a)SPP-BAF and (b)SPP-BP

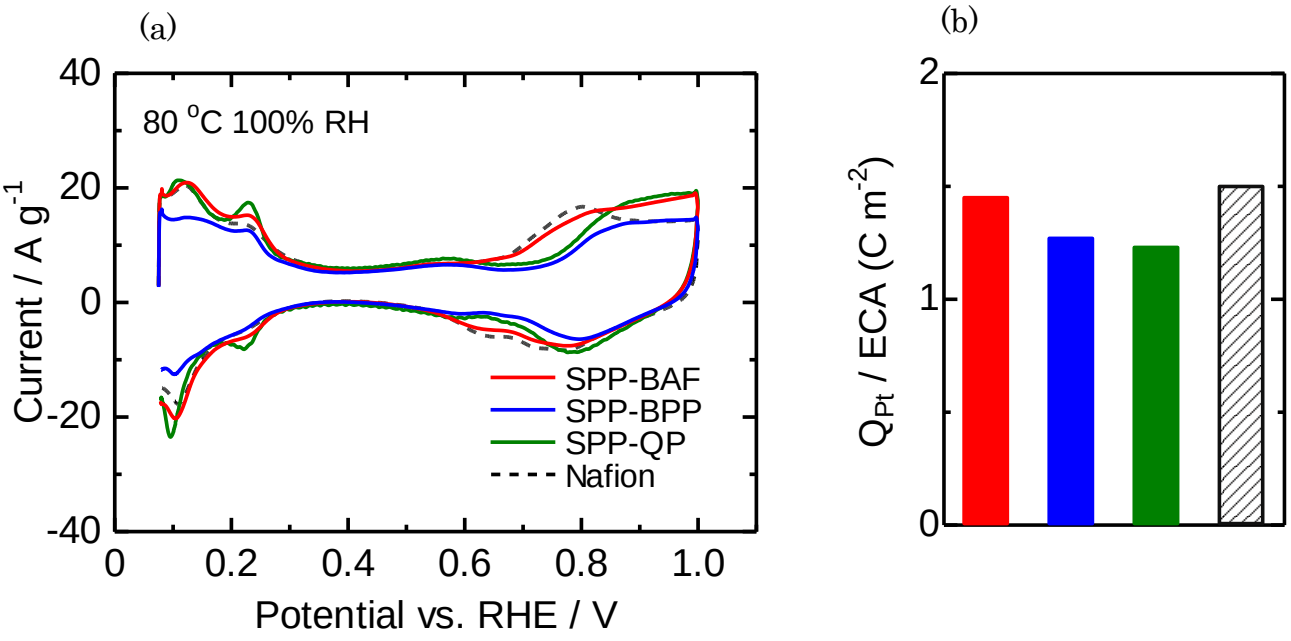

Figure 4-3 (a) CV, (b) Q_{Pt} / ECA of cells using SPP-BAF, SPP-BPP, SPP-QP or Nafuion as cathode binder at 80 °C 100% RH

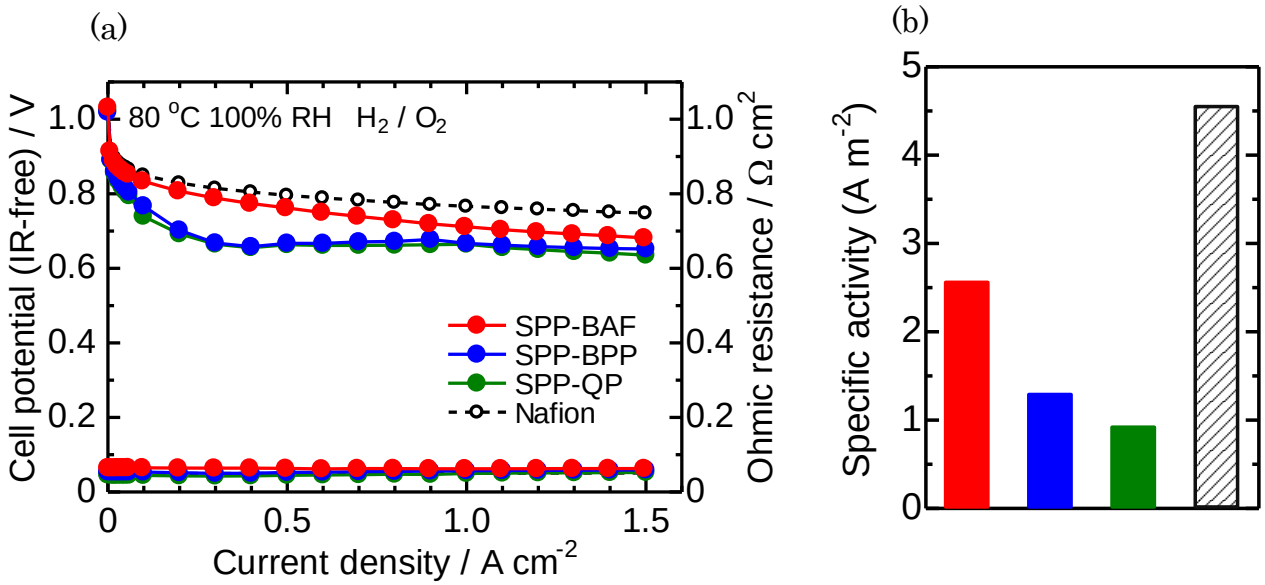

Figure 4-4 (a) Polarization curve and ohmic resistance (b) specific activity of cells using SPP-BAF, SPP-BPP, SPP-QP or Nafion as cathode binder at 80 °C 100% RH.

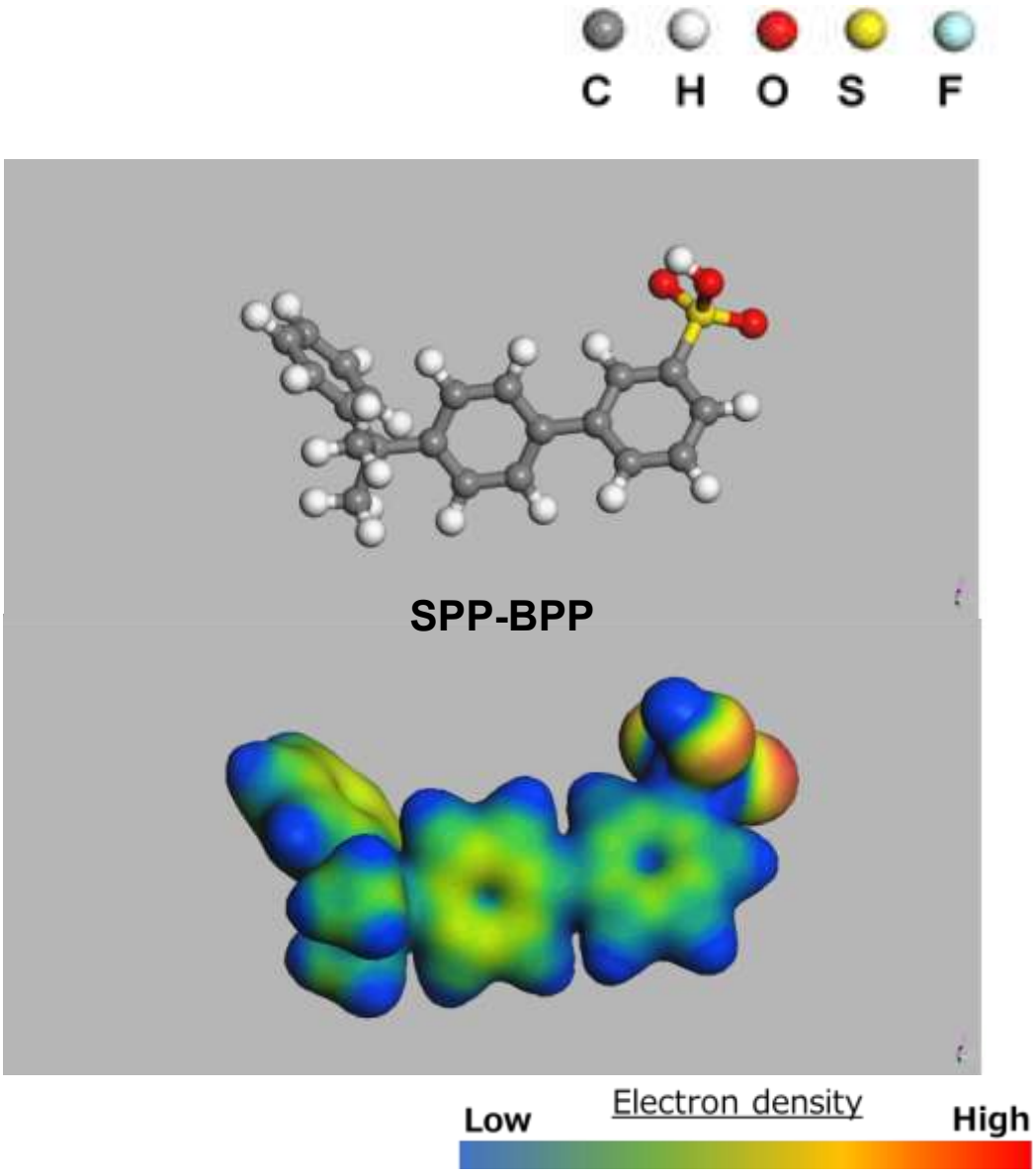
C H O S F
SPP-BPP
Low
Electron density
High

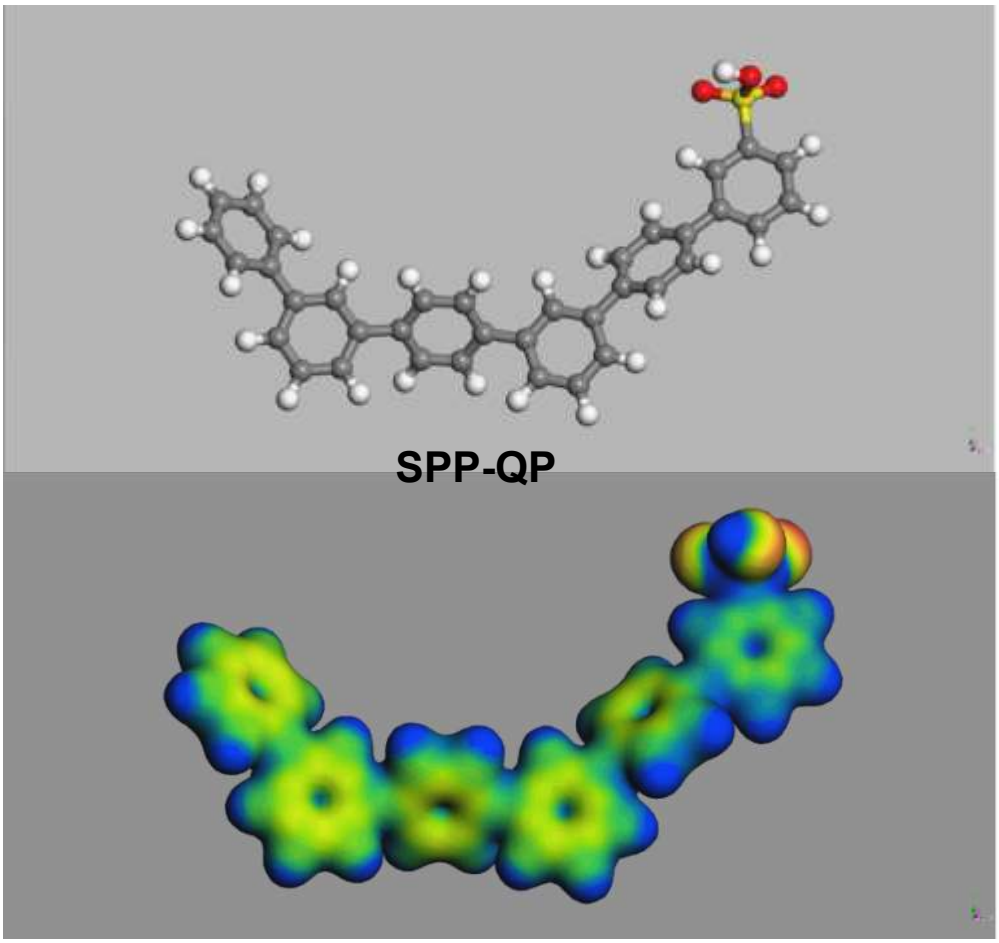
SPP-QP

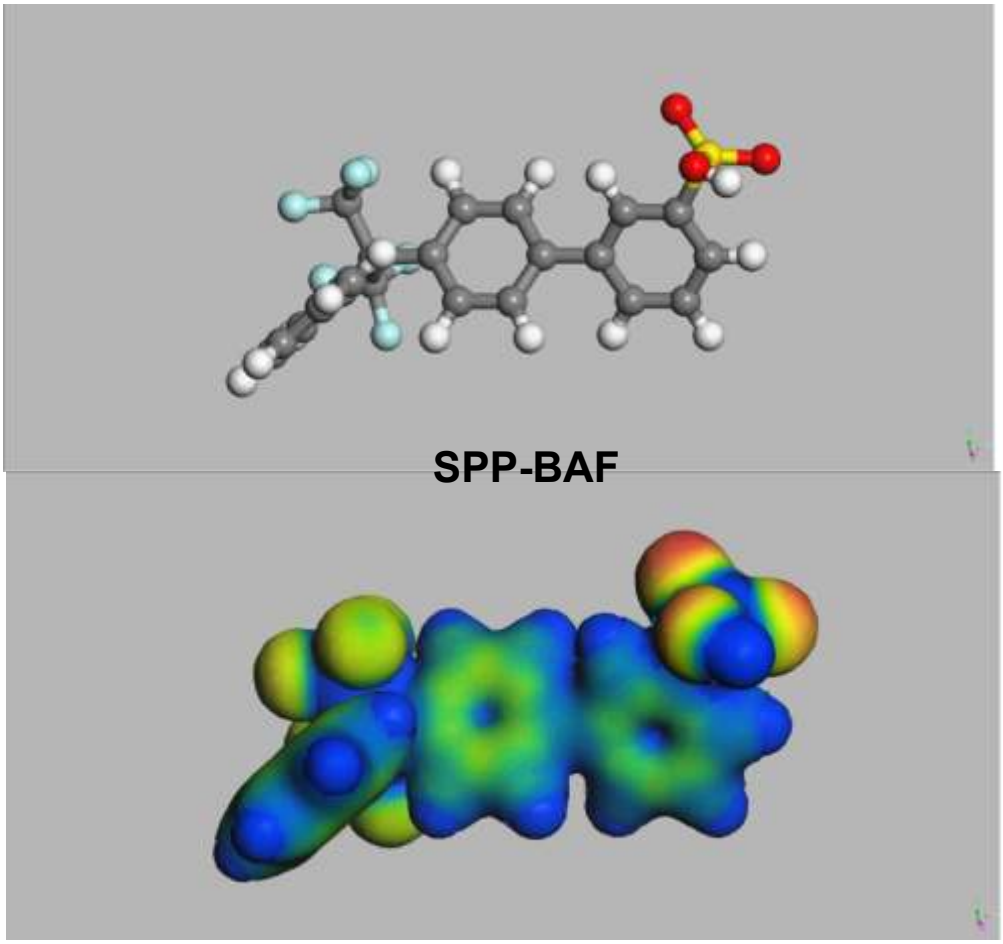

Figure 4-5 Electron density distribution of optimized molecular structure calculated by DFT

Another issue is that HC electrolytes generally have a high gas barrier property, so it is necessary to improve the permeability of gas (especially oxygen). To solve this problem, I focused on the bulky structure shown in Figure 4-6. Figure 4-6 shows the cell performance using an electrolyte with or without this structure as the cathode binder. The bulky structure of the SPP-BAF-cHx cell showed higher performance than the SPP-BAF cell in the high current density region, which is greatly affected by gas mass transport. In addition, this

difference was large when air was used as the cathode fuel. This result suggests that the bulky structure may improve the gas permeability of the electrolyte. Further structural/properties analyses will be needed to understand better the effect of such bulky cyclic structure on the mass transport capability of this emerging ionomer.

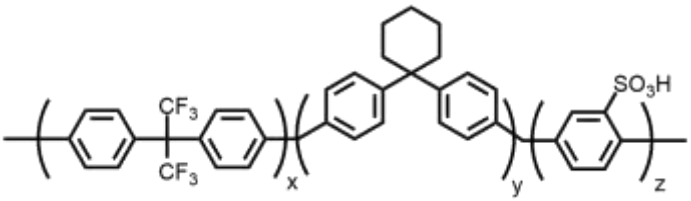

SPP-BAF-cHx

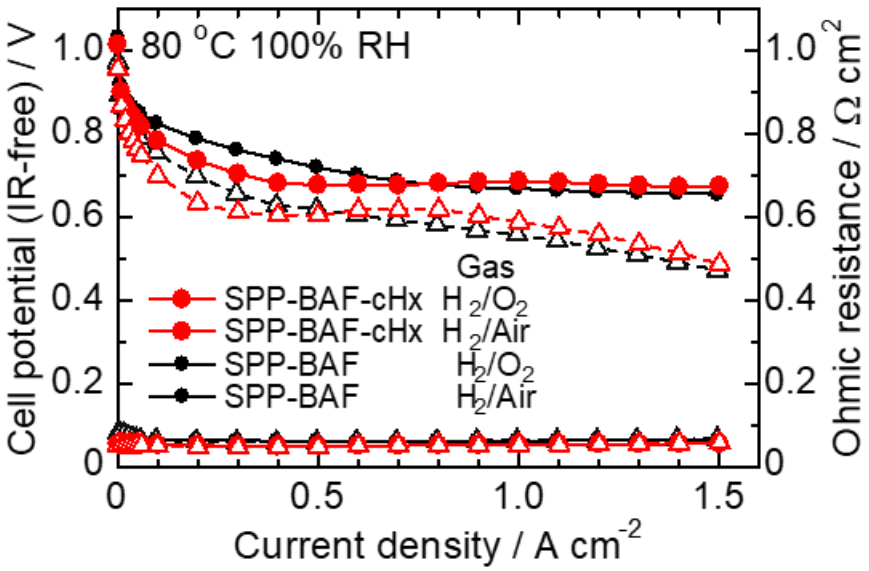

Figure 4-6 Polarization curve of cells using SPP-BAF or SPP-BAF-cHx as cathode binder at 80 ºC 100% RH.

Figure 4-7 shows the cell evaluation results of cells using SPP-QP and cells using Nafion for all electrolytes. From the CV in Fig. 4-7 (a), the Pt redox quantity of the all SPP-QP cell was smaller, because the SPP-QP binder prevented the activity of Pt. In Figure 4-7 (b), the resistance of the all SPP-QP cell is higher than that of the all Nafion cell. This result means that the proton conduction between the membrane and the binder is not good. Generally, the glass transition temperature of the polyphenylene is over 200 ºC, but the temperature of the hot press is 140 °C, so the conditions may be insufficient. It is also important to consider the manufacturing conditions when using HC electrolytes. In addition, the performance of the all SPP-QP cell was very low. The use of HC electrolytes in the membranes and electrolytes may have caused factors that further reduced performance (water management, etc.). This is a topic for future study of all HC electrolyte cells. There are still many problems that must be solved in order to use HC electrolytes as electrolytes for PEFCs, but if these are cleared, the high thermal stability of HC electrolytes will make them promising ion-conducting binders for high-temperature operation. Finally, Table 4-1 summarizes the benefits and challenges of HC electrolytes for fuel cell applications.

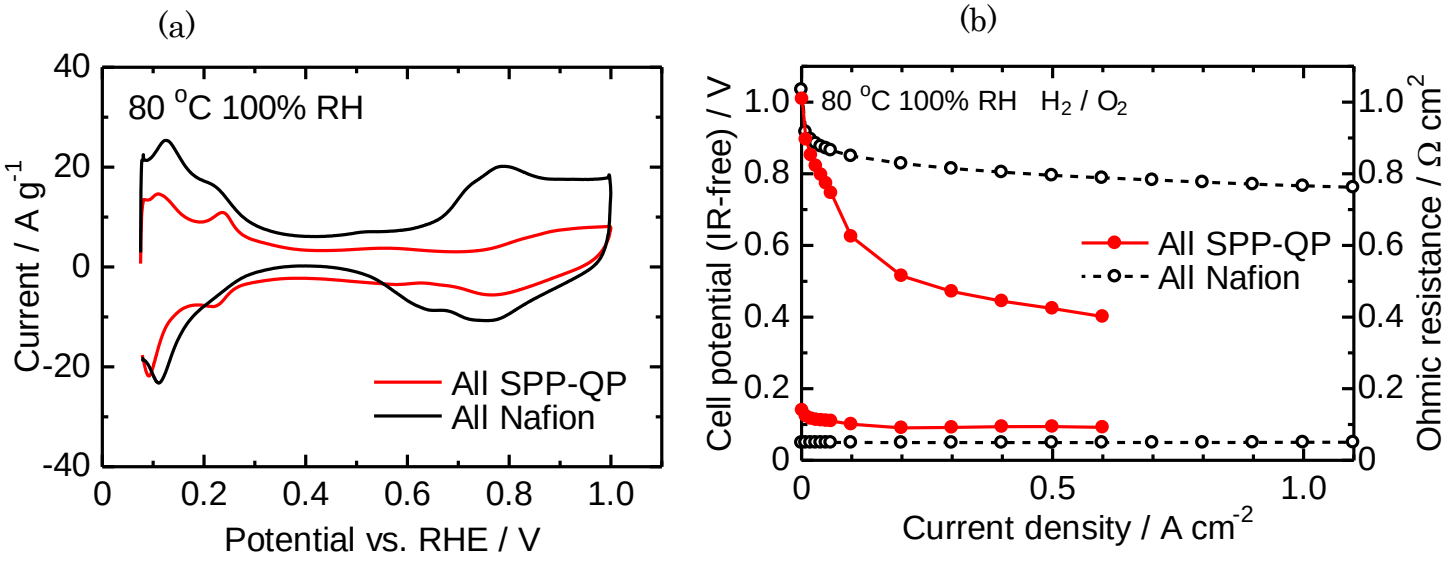

Figure 4-7 (a)CV and polarization curve of cells all SPP-QP cell or all Nafion cell at 80 °C 100% RH.

Table 4-1 The advantages and current challenges of HC electrolytes.

	Proton conductivity	Cost	Chemical stability	Thermal stability	Mechanical stability	Gas permeability	Specific adsorption
HC electrolyte	○	○	◎	◎	△	Membrane ◎ Binder △	△
Perfluorinated electrolyte	◎	△	○	△	◎	Membrane △ Binder ○	○

4.3 Feasibility

Widespread use of PEFCs and the realization of a hydrogen-based society are indispensable for solving current energy and environmental problems. To that end, it is important to (1) reduce costs and (2) improve the reliability and durability of the devices. (1) Regarding the cost reduction, Figure 4-8 shows the cost distribution of the PEFC stack estimated by the US Department of Energy. The electrolyte membrane accounts for 12% of the total cost. This is due to the complicated synthetic route of perfluoro polymer electrolytes. The target cost of the electrolyte membrane is 2000 yen / m^2 or less, but the price of the perfluorinated electrolyte currently in use is 561,900 yen / m^2. [2-3] Although the mass production effect would significantly reduce the product cost, the target does not seem feasible for the perfluorinated ionomers. Most HC electrolytes can be synthesized and manufactured via a simple synthetic route, so the production cost can be reduced. Currently, the use of costly polymerization catalysts is used, therefore, developing new synthetic routes and catalysts is a must. (2) Regarding the improvement of reliability and durability, Fig. 4-9 summarizes the causes of the deterioration of PEFC under various operating conditions. [4-5] Startup-Stop degradation is 33%, the second highest following the load fluctuations. This study revealed that the use of HC electrolyte as the anode binder mitigated start-up-stop deterioration. There are many studies for improving startup-stop durability, but most of them are related to the catalysts and operating methods, and few focus on binders. Therefore, the new insight

obtained in this study should be applied to emerging catalysts and catalyst supports with more robustness for further prolonging the total lifetime of PEFCs.

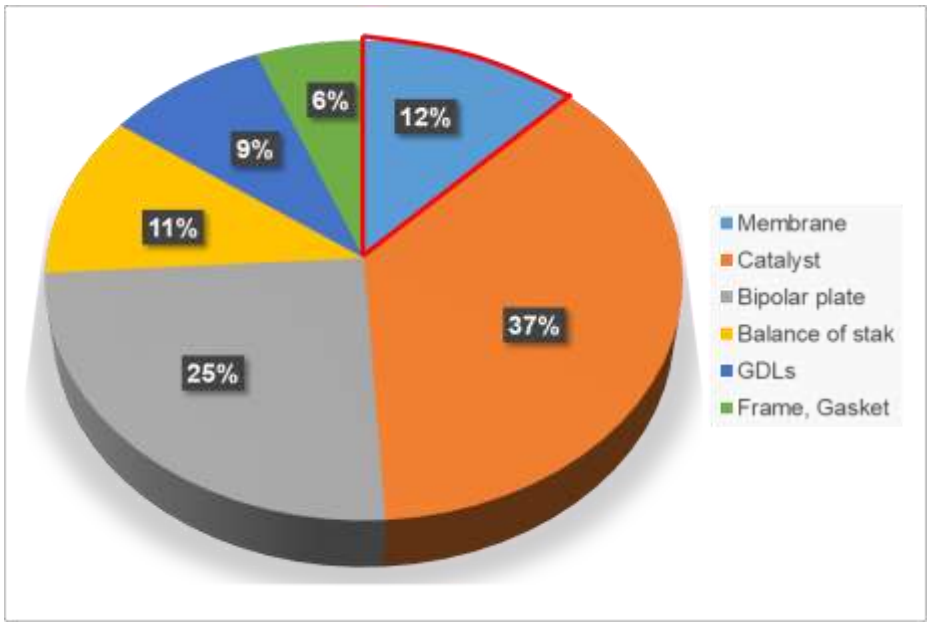

Figure 4-8 Cost distribution of PEFC stack.

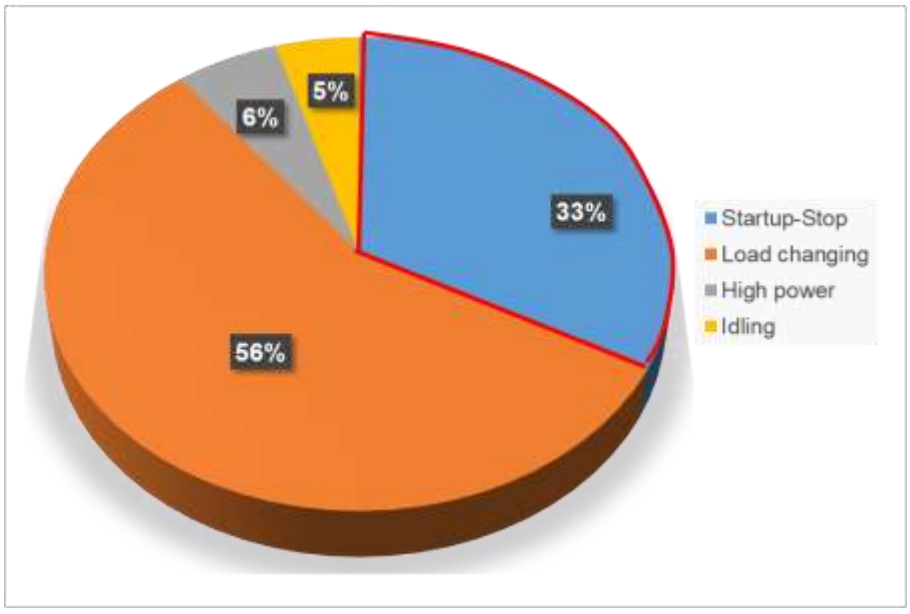

Figure 4-9 Percentage of degradation causes under various operating conditions of PEFC

4.4 References

1. J. Miyake, T. Watanabe, H. Shintani, Y. Sugawara, M. Uchida, and K. Miyatake, *ACS Mater. Au,* 1 (2021) in press.
2. MerckHP https://www.sigmaaldrich.com/catalog/product/aldrich/676470?lang=ja&region=JP
3. NanotechJapan Bulletin Vol. 7, (2014), No. 4.
4. H. Chena, X. Zhao, T. Zhang, P. Pei, *Energy Convers. Manag.* **182** (2019) 282– 298.
5. P. Pei, Q. Chang, T Tang, **33** (2008) 3829–3836.

List of publication

1. Wet/Dry Cycle Durability of Polyphenylene Ionomer Membranes in PEFC

T. Tanaka, H. Shintani, Y. Sugawara, A. Masuda, N. Sato, M. Uchida, and K. Miyatake

J. Power Sources Adv., **10** (2021), 100063

2. Aromatic Ionomer in the Anode Catalyst Layer Improves Start-up Durability of Polymer Electrolyte Fuel Cells

T. Tanaka, M. Uchida, and K. Miyatake, *Energy Adv.*, **1,** (2021) 38.

Meeting abstracts

1. 6th International seminar on green energy conversion, Nagano, Japan (2017.7)

   Toshiki Tanaka, Makoto Uchida, and Kenji Miyatake

   22nd Topical Meeting of the International Society of Electrochemistry, Tokyo, Japan(2018,3), Toshiki Tanaka, Makoto Uchida, and Kenji Miyatake

2. 7th International seminar on green energy conversion, Kofu, Japan (2018.8)

   Toshiki Tanaka, Makoto Uchida, and Kenji Miyatake

3. The 8th International Fuel Cell Workshop, Kofu, Japan (2018.8)

   Toshiki Tanaka, Makoto Uchida, and Kenji Miyatake

4. 68th SPSJ Annual Meeting, Osaka, Japan (2019, 5)

   Toshiki Tanaka, Makoto Uchida, and Kenji Miyatake

5. 9th International seminar on green energy conversion, Kofu, Japan (2019.10)

   Toshiki Tanaka, Makoto Uchida, and Kenji Miyatake

6. 60th Battery symposium in Japan, Kyoto, Japan (2019, 11)

Toshiki Tanaka, Makoto Uchida, and Kenji Miyatake

Acknowledgments

This thesis is the summer of research at the Fuel Cell Nanomaterials Center and clean Energy Research Center, the Integrated Graduate School of Medicine, Engineering, and Agricultual Sciences at the University of Yamanashi, during 2017-2022. This research was supported by funds for the "Superlative, Stable, and Scalable Performance Fuel Cell" (Sper-FC) project from the New Energy and Industrial Technology Development Organization (NEDO).

I would like to express my deepest gratitude to **Professor Kenji Miyatake** of University of Yamanashi for this academic supervisor of this work, for his continuous guidance, invaluable suggestion, and warm encouragement thought the study.

I would like to express my gratitude to Associate **Professor Makoto Uchida** and **Professor Katsuyoshi Kakinuma** of University of Yamanashi for continuous supports, beneficial instructions and invaluable help and advices.

I would like to express my gratitude to **Professor Hiroyuki Uchida** and **Professor Akihiro Iiyama** of University of Yamanashi for warm encouragements, continuous consideration and kindness.

I would like to thank **Professor Junji Inukai**, and **Associate Professor Takuji Oyama** of University of Yamanashi, and **Professor Hiroyoshi Kawakami** of Tokyo Metropolitan University for the helps as members of the advisory committee.

I would like to express my sincere graduate to **Professor Donald Alexander Tryk, Professor Toshihiro Miyao, Professor Kazuhiro Higashiyama, Professor Takeo Kamino, Professor Tomio Omata, Professor Manuel Eduardo Brito, Associate Professor Shinji Noahara, Associate Professor Junppei Miyake, Associate Professor Mitsuru Wakisaka, Associate Professor Hiroshi Yano, Associate Professor Hanako Nishino, Associate Professor Teppei Kawamoto** of the University of Yamanashi, for valuable support and professional guidance.

I am grateful to **Dr. Akinobu Matsumoto, Dr. Ryo Akiyama, Mr Toshio Iwataki, Mr. Takahiro Asakawa, Ms. Toshiko Gomyo, Ms. Mika Kodama, Ms. Setsuko Mori, Ms Kayoko Tamoto Ms. Miho Yamaguchi** for technical supports and practical discussions.

I would like to thank **Dr. Yuya Yamashita, Dr. Ryo Shimizu, Dr. Hideaki Ohno, Dr. Ibuki Hosaka, Dr. Taro Kimura, Mr. Naoki Hirayama, Dr. Keisuke Shiino, Dr. Yu**

Kakizawa,Mr. Ueno Koki, Ms. Mizuki Hayashi, Dr. Hiromichi Nishiyama, Ms. Aki Kobayashi, Mr. Ryo Kobayashi, Mr. Takahiro Matsumoto, Mr. Daiki Hasegawa, Mr. Syunsuke Ishikawa, Mr. Takeshi Kawamura, Mr. Junya Yamada, Mr. Takayuki Watanabe, Mr. Shinichiro Tsutsui, Mr. Kodai Kitagawa, Mr. Yuki Miyamoto, Mr. Naoki Ogawa, Mr. Takumi Hashimoto, Mr. Yuto Shirase, Mr. Takumi Nagasaka, Mr. Yasuaki Ogawa, Mr. Masaaki Ito, Mr. Ren Kumao, Mr. Makoto Yonenaga, Mr. Masato Shikano, Mr. Yoshihiro Ozawa, Mr. Ryohei Tomiyama, Mr. Ryuji Ohno, Ms. Sayaka Takahashi, for their kindly support.

I would like to thank **Dr. Takashi Mochizuki, Dr. Yuii Chino, Dr. Kazuhiro Takanohashi, Dr. Manai Shimada, Dr. Hideaki Ono, Dr Katsuyuki Hagiwara, Dr. Kento Takahashi, Dr. Ryosuke Nishikawa, Dr. Shun Kobayashi, Mr. Ichiro Nagata, Mr. Seiya Kosaka, Mr. Yuma Shimizu, Mr. Shinya Hanyu, Mr. Ryo Shirasaka, Mr. Kohei Uyama, Mr. Yuta Oishi, Ms. Rutsu Tamura, Mr. Takatoshi Sawano, Mr. Takashi Sato, Dr. Zhang Yaojian, Dr. Zhi Long, Dr. Jinju Ahn, Ms. Liu fanghua, Mr. Guo Lin,** for their grateful support.

Sincere gratitude is also expressed to **Ms. Nozomi Toyoda, Ms. Tomomi Hashizume** and all staffs of Fuel Cell Research Nanomaterials Center, Clean Energy Research Center for their kind support and help.

I greatly appreciate the support of my family, **Matsuichiro Tanaka, Etsuko Tanaka, and Hiroki Tanaka** to their support and sincere encouragement.

Toshiki Tanaka

March 2022